Estimating the disequilibrium in denudation rates due to divide migration at the scale of river basins.

Timothée Sassolas-Serrayet[1], Rodolphe Cattin[1], Matthieu Ferry[1], Vincent Godard[2], Martine Simoes[3]

[1]Géosciences Montpellier, Université de Montpellier ~~and~~ , CNRS ~~UMR 5243~~, Montpellier ~~34095~~, France.
[2]Aix Marseille Univ, CNRS, IRD, INRA, Coll France, CEREGE, Aix-en-Provence, France
[3]Université de Paris, Institut de physique du globe de Paris, CNRS, F-75005 Paris, France

Correspondence to: Timothée Sassolas-Serrayet (timothee.sassolas-serrayet@umontpellier.fr)

Abstract. Basin-averaged denudation rates may locally exhibit a wide dispersion, even in areas where the topographic steady state is supposedly achieved regionally. This dispersion is often attributed to the accuracy of the data or to some degree of natural variability of the signal~~, but it~~, which can ~~also~~ be ~~attributed~~related to stochastic processes such as landsliding. Another physical explanation to this dispersion is that of local and transient disequilibrium between tectonic forcing and erosion at the scale of catchments. Recent ~~works~~studies have shown that divide migration can potentially induce such perturbations and they propose reliable metrics to assess divide mobility based on cross-divide contrasts in headwater topographic features. Here, we use a set of landscape evolution models assuming spatially uniform uplift, rock strength and rainfall to assess the effect of divide mobility on basin-wide denudation rates. We propose the use of basin-averaged aggressivity metrics based on cross-divide contrasts (1) in channel~~-head~~ χ, an integral function of position in the channel network, (2) in channel local ~~slope~~gradient and ~~in elevation.~~(3) in channel height, measured at a reference drainage area. From our simulations, we show that the metric based on differences in ~~channel-head elevations across divides~~ χ is the ~~least~~most reliable to diagnose local disequilibrium. ~~For the~~The other metrics~~, our results suggest a nonlinear relationship with~~ are more suitable for relatively active tectonic regions as mountain belts, where contrasts in local gradient and elevation are more important. We find that the ratio of basin denudation associated with drainage migration to uplift~~, which~~ can reach ~~up to~~ a factor of two, regardless ~~of~~ the imposed uplift rate, erodibility, diffusivity coefficient and critical hillslope gradient. A comparison with field observations in the Great Smoky Mountains (southern Appalachians, USA) underlines the difficulty of using the metric based on ~~χ~~ χ, which depends on the -~~-~~poorly constrained~~-~~- elevation of the outlet of the investigated catchment. Regardless ~~of~~ the considered metrics, we show that observed dispersion is controlled by catchment size: a smaller basin may be more sensitive to divide migration and hence to disequilibrium. Our results thus highlight the relevance of divide stability analysis from digital elevation models as a fundamental preliminary step for basin-wide denudation rate studies based on cosmogenic radionuclide concentrations.

Mis en forme: Anglais (États Unis)

Mis en forme: Français (France)

Mis en forme: Français (France)

Mis en forme: Anglais (États Unis)

Mis en forme: Anglais (États Unis)

Mis en forme: Police :Gras, Anglais (États Unis)

Mis en forme: Anglais (États Unis)

1 Introduction

Topographic steady state, in which average topography is constant over time, is one of the key concepts of modern geomorphology (e.g. Gilbert, 1877; Hack 1960; Montgomery, 2001). Though simple, this paradigm provides a useful framework to study landscape evolution related to tectonic and/or climatic forcing (e.g. Willett et al., 2001; Reinhart and Ellis, 2015), to spatial variations in rock strength (Perne et al., 2017) or to the geometry of active crustal structures (Lave and Avouac, 2001; Stolar et al., 2007; Scherler et al., 2014; Le Roux-Mallouf et al., 2015). To define topographic steady state, the temporal and spatial scales of the processes involved are essential parameters. Compared to large scale geodynamic processes operating over 1-100 Myr timescales, river incision and sediment transport are rapid processes driving landscapes to stable forms over this long timescale, whereas rapid climatic fluctuations during the Quaternary may prevent ~~modern landscapes from reaching~~the occurrence of steady-state conditions in modern landscapes (Whipple, 2001).

The timescale of river divide migration has received increasing attention in the recent years. Although rivers exhibit a rapid adjustment to tectonic or climatic changes to maintain their profiles, Whipple et al. (2017) show that divides continue to migrate over time periods of 10^6-10^7 years~~, suggesting~~ as response to the same changes. This suggests that long-term transience might be pervasive in the planar structure of landscapes, even in the absence of new variations in landscape characteristics or forcings (e.g. tectonic or climate) (Hasbargen and Paola, 2000; Hasbargen and Paola, 2003; Pelletier, 2004, Dahlquist et al., 2018). In addition to the influence of spatial variability of rock uplift rate, rock strength or rainfall (e.g. Reiner et al., 2003; Godard et al., 2006; Miller et al., 2013), this long timescale could also explain the persistence of spatial variations in denudation rates observed in tectonically inactive orogens in spite of a supposedly and theoretically topographic achieved steady state~~ is achieved~~ (Willett et al., 2014).

As an example~~ of this~~, in the Great Smoky Mountains in the southern Appalachians, uplift and erosion rates integrated over varying time periods from 10s kyr to 100 Myr give a similar average magnitude of ~~0.025-0.030 mm.yr^{-1}.~~ca. 0.03 mm.yr^{-1} (Matmon et al., 2003a, b and Portenga and Bierman, 2011). These results suggest a regional quasi-topographic steady state over the last ~180 Myr, maintained by the isostatic response of the thickened crust since the end of the Appalachian orogeny (Matmon et al., ~~2003 a,~~2003a, b). Beyond this average value, individual basin-wide denudation rates exhibit a strong dispersion (up to a factor of two, Fig. 1), which is not related to spatial variation in rainfall or in erodibility of the substrate (Matmon et al., 2003b). In a recent study, Willett et al. (2014) assess divide mobility from the contrast in the channel head topographic metric χ, taken here as a proxy for steady-state river profile elevation (Perron and Royden, 2012; Royden and Perron, 2013), and propose an explanation in which a significant part of the observed dispersion in denudation rates could be due to drainage divide migration associated with contrasting erosion rates across divides.

~~Divide migration is often assessed through the metric χ (Willett et al, 2014).~~ More recently, to characterize divide migrations Forte and Whipple (2018) introduced other metrics, referred as "Gilbert metrics" (Gilbert, 1877), based on the cross-divide contrast in channel head local ~~slope~~gradient and elevation~~ in order to characterize divide migrations.~~. This last study indeed focused on cross-divide contrasts in headwater basin shape. Here, we ~~model divide migrations and~~ propose to extend these

Mis en forme: Anglais(États Unis)

approaches by modeling divide migration and by developing new metrics ~~of~~to assess divide stability at the scale of the entire watershed, which are an expansion of the aggressivity metric initially suggested by Willett et al. (2014). We use these metrics to assess the effect of persistent divide mobility on basin-averaged erosion rates at a timescale of 10^4 yr. We use numerical landscape evolution models, taking into account both hillslope diffusion and fluvial incision. For the sake of simplicity and to avoid the influence of other factors such as topography, lithology, climate or vegetation, we restrict our analysis to synthetic orogens with spatially uniform uplift, rock strength and rainfall. After a brief presentation of the used landscape evolution model (LEM), we describe the methods developed to assess basin-wide denudation rates and aggressivity metrics, such as average cross-divide contrasts in ~~headwater~~channel χ, ~~slope~~gradient and elevation. Next, we investigate transient time and location of morphologic adjustments to divide migrations. We explore the relevance and complementarity of tested relative stability metrics between ~~neighbouring~~neighboring basins. We then investigate the impact of uplift rate, erodibility and hillslope ~~process~~processes on the dynamics of divide migration and associated denudation rates. Finally, we apply our approach to the basin-wide denudation rates dataset of Matmon (2003a,b) in the case of the Great Smoky Mountains and propose new criteria to guide future sampling strategies to assess basin-wide denudation rates from river sands.

2 Methods

2.1 Landscape Evolution Model (LEM)

We use TTLEM (TopoToolbox Landscape Evolution Model) (Campforts et al., 2017), a landscape evolution model based on the Matlab function library TopoToolbox 2 (Schwanghart and Scherler, 2014). This LEM uses a finite volume method (Campforts and Govers, 2015) to solve the following equation of mass conservation for rock/regolith subject to uplift and denudation:

$$\frac{\partial z}{\partial t} = \left(\frac{\partial z}{\partial t}\right)_{td} + \cancel{\begin{cases} U + \left(\frac{\partial z}{\partial t}\right)_{fluv} & \text{for } A < A_c \\ \frac{\rho_r}{\rho_s}U + \left(\frac{\partial z}{\partial t}\right)_{hill} & \text{for } A < A_c \end{cases}} \frac{\rho_r}{\rho_s} U + \left(\frac{\partial z}{\partial t}\right)_{hill} + \left(\frac{\partial z}{\partial t}\right)_{fluv} ,$$

(1)

where $\partial z/\partial t$ is the variation of elevation with time, $(\partial z/\partial t)_{td}$ is the change of elevation due to tectonic horizontal advection, U is the rock uplift rate~~-~~, ρ_r/ρ_s is the density ratio between the bedrock and the regolith~~, A is the upstream area and A_c is~~. We use a linear formulation of hillslope diffusion (Culling, 1963) limited by a critical ~~drainage area which corresponds to the transition between hillslope and fluvial processes.~~ slope S_c:

~~Hillslope denudation is given by a non-linear formulation (Roering et al., 1999):~~

Mis en forme: Anglais(États Unis)
Mis en forme: Anglais(États Unis)
Mis en forme: Anglais(États Unis)
Mis en forme: Anglais(États Unis)
Mis en forme: Anglais(États Unis)
Mis en forme: Anglais(États Unis)
Mis en forme: Anglais(États Unis)
Mis en forme: Anglais(États Unis)

$$\left(\frac{\partial z}{\partial t}\right)_{hill} = -\nabla q_s \quad \text{with} \quad q_s = -\cancel{\frac{D\nabla z}{1-\left(\frac{|\nabla z|}{S_c}\right)^2}} D\nabla z, \tag{2}$$

where q_s is the flux of soil-regolith material. ~~This flux rate increases to infinity when slope tends to a critical value S_c.~~When slopes values exceed S_c, they are readjusted to the critical value by using a modified version of the excess topography algorithm (Blöthe et al., 2015). The diffusivity D gives the rate of soil-regolith material creep. Its magnitude ranges from 10^{-3} to 10^{-1} m².yr^{-1} in natural settings and varies with soil thickness, lithology and vegetation (Roering et al., 1999; Jungers et al., 2009; West et al., 2013; Richardson et al., 2019). Hillslope diffusion is implemented in TTLEM using an implicit scheme, which is unconditionally stable at large time steps (~~Perron, 2011).~~ Pelletier, 2008). Non-linear diffusion formulation (Perron, 2011) is also implemented in TTLEM. However, we favored the use of a linear diffusion with a critical slope, which is more convenient for the time step used in our simulations (=5000 yr) and the set of parameters considered (see section **2.2**). Due to the relatively coarse spatial resolution of our models (= 90m), any of these diffusion formulations generate negligible topographic differences on the direct vicinity of crest lines (Roering et al., 1999, Campforts et al., 2017) and do not affect our results (see Fig. S1). Fluvial incision is calculated with a stream power law:

$$\left(\frac{\partial z}{\partial t}\right)_{fluv} = -KA^m\left(\frac{\partial z}{\partial x_r}\right)^n, \tag{3}$$

where K ~~is~~Is the erodibility coefficient reflecting climate, hydraulic roughness, sediment load and lithology. Its value ranges between 10^{-16} and 10^{0} m$^{(1-2m~~)~~)}$ .yr^{-1} (Kirby and Whipple, 2001; Harel et al., 2016). A is the upstream area. x_r is the along stream distance from the outlet of the river. m and n are two parameters ~~which~~that are usually reported as a m/n ratio ranging between 0.35 and 0.8. ~~River~~The river incision law is implemented in TTLEM using an explicit scheme based on a higher-order flux-limiting finite volume method that is total variation diminishing (TVD-FVM) [see Campforts and Govers (2015) and Campforts et al. (2017) for further details]. Its main advantage is to eliminate numerical diffusion, which is present in most other schemes solving differential equations of river incision. This last point has a significant impact on the accuracy of basin-wide simulated denudation rates~~.~~, making TTLEM a well-suited LEM for the purpose of this study.

Mis en forme: Anglais(États Unis)

Mis en forme: Anglais(États Unis)

Mis en forme: Anglais(États Unis)

Mis en forme: Exposant

Mis en forme: Anglais(États Unis)

Mis en forme: Anglais(États Unis)

Mis en forme: Anglais(États Unis)

Mis en forme: Anglais(États Unis)

Mis en forme: Anglais(États Unis)

Mis en forme: Anglais(États Unis)

2.2 Modeling approach and assumptions

2.2.1 Geometry and meshing

Since the computation is performed using a discretized land surface, smaller mesh sizes ~~will~~ lead to detailed topography but ~~will~~ lengthen the computation time and memory requirements. Hereinafter, we consider a reference square landscape model of 50 km side with a grid resolution of 90 m, which is a good compromise between computation time (3-5 hours on a PC workstation) and the total amount of basins that can be studied (>1000). Our results are not affected when the ~~mesh~~grid resolution is ~~increased to~~ 30 m nor ~~are they~~ when the model size is ~~multiplied by four (~~100x100 km~~) (See~~ (see Fig. ~~S1~~S2).

2.2.2 Boundary conditions

In order to isolate the effect of divide migrations on the variability of basin-wide denudation rates, we explore simple models with constant and spatially uniform uplift and precipitation rates and we assume no horizontal advection $(\partial z/\partial t)_{td} = 0$. We use a Dirichlet boundary condition: simulation edges are not affected by uplift on a one pixel band to represent a stable base level for rivers. The model presents no initial topography, except for gaussian noise ranging between 0 and 50 m so as to initiate a random fluvial network.

2.2.3 Set of parameters

Firstly, we consider a reference model with parameters commonly used for moderately active orogens: an uplift rate U of 0.1 mm.yr^{-1}, a diffusivity D of 10^{-2} m^2.yr^{-1} (Roering et al., 1999), a threshold slope S_c of 30° (Burbank et al., 1996; Montgomery et Brandon, 2002; Binnie et al., 2007), a m/n ratio of 0.5 with $m = 0.5$ and $n = 1$, an erodibility coefficient K of ~~5x10^{-6} m^{-1}~~1x10^{-5} m$^{(1-2m)}$~~;~~.yr^{-1}, a ρ_r/ρ_s ratio of 1.3~~ and a critical drainage area A_c of 0.2 km² (Montgomery et al., 1993).~~.
Secondly, all other parameters held constant, we investigate the specific impact of uplift rate, erodibility and hillslope processes in other models by varying U, K, D and S_c between 0.~~5~~01 and ~~2~~1 mm.yr^{-1}, 5.10^{-5} m$^{(1-2m)}$.yr^{-1}and 5.10^{-6} m$^{(1-2m)}$.yr^{-1}, 10^{-3} and 10^{-1} m^2.yr^{-1} and 20° and 40°, respectively.
In order to better constrain the variability of our results under similar conditions, we run for each model five simulations using the same parameters, but with different initial random topographies.

2.2.4. Timescale

The total duration of simulations is 10 Myr~~, which is nearly one order of magnitude longer than the theoretical time to reach general topographic equilibrium for our set of parameters (Willett, 2001).~~. The implicit scheme used to simulate ~~non-~~linear hillslope processes provides stable solutions regardless of the time step. In contrast, the explicit scheme used to model fluvial incision requires a time step that satisfies the Courant-Friedrich-Lewy criterion. Hereinafter, we choose a time step Δt of ~~500~~5000 yr for hillslope diffusion. Our results are not affected when using a smaller Δt (i.e. 1000 yr) (see Fig. S1). Incision

Mis en forme: Anglais(États Unis)
Mis en forme: Anglais(États Unis)
Mis en forme: Anglais(États Unis)
Mis en forme: Anglais(États Unis)
Mis en forme: Anglais(États Unis)
Mis en forme: Anglais(États Unis)
Mis en forme: Anglais(États Unis)
Mis en forme: Anglais(États Unis)
Mis en forme: Anglais(États Unis)
Mis en forme: Anglais(États Unis)
Mis en forme: Anglais(États Unis)
Mis en forme: Anglais(États Unis)
Mis en forme: Anglais(États Unis)
Mis en forme: Anglais(États Unis)

computation is nested in this time step and uses another time step that is automatically determined to assure model stability (Campforts et al., 2017).

2.3 Basin-wide denudation rates and aggressivity metrics

2.3.1 Basin-wide denudation rates

We derive basins from the synthetic DEMs (Digital Elevation Models) using an accumulation map computed with a single flow direction algorithm implemented in TopoToolbox (Schwanghart and Scherler, 2014). Next, we calculate for each basin the variation in average elevation over a time interval of 10 kyr~~, which averages the results over 20 time steps.~~. The drainage network ~~can migrate~~migrates during the simulation, so we only survey the basins that keep the same outlet location during this time interval. Furthermore, due to divide mobility, the geometry of watersheds can also change. Hence, we measure the average difference in elevation inside the basin perimeter after 10 kyr. Here we only assess the surface uplift U_s (England and Molnar, 1990). To ~~obtain~~approximate the ~~real~~ denudation rates E for each basin, we sum the surface uplift U_s with the rock uplift rate U ~~assumed in our simulation~~ and divide the result by the time interval~~, which is an approximation. However, calculating incremental denudation rates over each time step is prohibitive in terms of computation time for the number of extracted basins~~. By considering the relatively small period over which we integrate denudation (10 kyr), we then assume that these approximations have a negligible impact on the results ~~at first order. Calculated that way, the denudation rate~~. If the basin is in a topographic steady state, U_s is equal to zero and E is equal to the background uplift rate. Thus, a positive (negative) value of U_s traduce a deficit (an excess) of denudation. Calculated that way, E is sensitive to divide migration but also to transient features like knickpoints that migrate along the river network. In our simulations, knickpoints may develop due to (1) the dissection of the initial flat surface or (2) discrete drainage captures (see Sec. 3.1). We use the knickpointfinder algorithm implemented in TopoToolbox (Schwanghart and Scherler, 2014) to identify the affected basins.

2.3.2 From cross-divide metrics to basin averaged aggressivity metrics

Most recent studies have focused on the relationship between drainage divide mobility and headwater across-divide contrast in either χ, ~~slope~~gradient, elevation or local relief values (e.g. Whipple et al., 2017; Forte and Whipple, 2018). Here, in line with Willett et al. (2014, see Supp. Mat. therein) we focus on the specific influence of divide migration on denudation rates at the scale of the entire stream basin. Our approach aims to integrate cross-divide contrasts in drainage network properties along the entire basin perimeter. We then obtain basin-averaged aggressivity metrics that determine if a watershed is either growing or shrinking (Willett et al. 2014).

~~First we calculate χ, local slope and elevation map for each channel pixel. χ~~First, we assess χ, local topographic gradient G and height H of the drainage network at a reference drainage area A_{ref} (Fig. 2). Ideally, A_{ref} must be equal to the area at which channelization occurs (Forte and Whipple, 2018). However, it is challenging to locate the accurate position of channel

Mis en forme: Anglais(États Unis)

Mis en forme: Anglais(États Unis)

Mis en forme: Anglais(États Unis)

Mis en forme: Anglais(États Unis)

Mis en forme: Anglais(États Unis)

Mis en forme: Couleur de police : Noir

Mis en forme: Anglais(États Unis)

Mis en forme: Couleur de police : Noir

heads (Clubb et al., 2016). Hence, we use a constant value of A_{ref} set to 1 km². The parameter χ, is an integral function of position along the channel network (Perron and Royden, 2012) described by the equation~~-~~:

$$\chi = \int_{x_b}^{x} \left(\frac{A_0}{A(x)}\right)^{\frac{m}{n}} dx \ , \qquad (4)$$

where $A(x)$ is the upstream drainage area at the location x, A_0 is an arbitrary scaling area set to 1 km². The m over n ratio refers here to the reference concavity of an equilibrated river profile. Its value is set to 0.5 in accordance with the model parameters. For each independent drainage network, we integrate χ from the outlet x_b, located at the model boundary (< 1 m high), to the channel heads. ~~We then~~Local gradient is determined for each DEM pixel from its eight-connected neighbors. Height is simply extracted from the DEM.

Then, we calculate the difference ~~in channel-head χ, local slope~~of metrics ($\Delta\chi$, ΔG and ~~elevation~~ΔH) across ~~each first-order basin~~the segments of divide ~~segment. The~~shared by two reference basins. Finally, the aggressivity metric is ~~finally~~ obtained by averaging these ~~first-order~~ across-divide differences along the perimeter of each ~~extracted~~sampled basin (Fig. ~~S2~~2). This way, the sign of the aggressivity metric in a basin corresponds to the difference of the averaged value of considered metric ~~(Channel-head χ, slope or elevation~~difference ($\Delta\chi$, ΔG and ΔH) in this basin with respect to ~~his~~its neighbours. This method has the advantage to ponderate the weight of individual divide segments by the number of pixels they contain, and then to provide a robust assessment of the basin aggressivity. Aggressivity metrics based on χ, G and H are hereafter referred to as $\Delta\chi_{av}$, ΔG_{av} and ΔH_{av}, respectively. ~~, which provide an accurate assessment of the basin aggressivity~~However, due to topology issues, some parts of the perimeter of the sampled basins may be not shared by two reference basins (Fig. 2). We quantify this incompleteness by assessing the ratio of documented pixels over the total amount of pixel along the basin perimeter. We refer to this ratio as the "confidence index" CI, assuming that an higher CI is associated with a more robust basin aggresivity assessment.

3 Results

3.1 Evolution of reference model

A detailed analysis of the DEM suggests that during the initial phase, the flat initial surface (Fig.~~2a~~3a) is progressively uplifted to form a plateau. At the same time the edges of this plateau are gradually regressively eroded by drainage networks that spread from the base level toward the center of the model (Figs. ~~2b~~3b and c). This transient landscape is completely dissected after 2 Myr. From this time and until the end of the simulation, landscape changes are mainly due to competition between watersheds, resulting in continuous divide migrations with decreasing intensity as the model is moving toward a total topographic equilibrium (Fig. ~~2d~~3d to f; Supplementary Video n°1).

Mis en forme: Anglais(États Unis)
Mis en forme: Anglais(États Unis)
Mis en forme: Anglais(États Unis)
Mis en forme: Anglais(États Unis)
Mis en forme: Anglais(États Unis)
Mis en forme: Anglais(États Unis)
Mis en forme: Anglais(États Unis)
Mis en forme: Anglais(États Unis)
Mis en forme: Anglais(États Unis)
Mis en forme: Anglais(États Unis)
Mis en forme: Anglais(États Unis)
Mis en forme: Anglais(États Unis)
Mis en forme: Anglais(États Unis)
Mis en forme: Anglais(États Unis)
Mis en forme: Anglais(États Unis)
Mis en forme: Anglais(États Unis)
Mis en forme: Anglais(États Unis)
Mis en forme: Anglais(États Unis)
Mis en forme: Anglais(États Unis)

~~We~~To define the time period of regional steady state, we measure the average elevation, the maximum elevation and the average denudation rate over the entire model for each time step (Fig. ~~3a) and~~4a). We identify two distinct stages during the evolution of our reference simulation. During the first million years, due to long wavelength topographic building, the calculated landscapes are far from steady state. This leads to a major increase of the mean elevation from 0 m to ca. ~~700~~75 m. In a second stage, this trend reverses and the mean elevation decreases asymptotically toward ca. ~~600~~60 m until the end of the simulation.

The evolution of the maximum elevation follows the same pattern but can be affected by temporal changes in the location and altitude of ~~higher~~highest peaks. The maximum elevation increases between 0 and ca. ~~2200~~250 m over the first ~~2 Myr (Figs. 3a~~3Myr (Fig. 4a) then decreases progressively to ~~reach~~remain at ca. ~~1600~~200 m ~~at~~during the ~~end~~rest of the simulation. We compute the average denudation rate from the ~~tectonic~~rock uplift rate and from average elevation change over the entire model between two time steps~~:~~:

$$(\Delta z/\Delta t)_{av} = U - E_{av} \,, \tag{5}$$

where ~~-~~$(\Delta z/\Delta t)_{av}$ is the average surface uplift over the entire model on a time-step Δt, U is the imposed uniform uplift rate (0.1 mm.yr^{-1}) and E_{av} is the average "real" denudation rate. During the first 0.25 Myr, the mean denudation rate falls abruptly from ca. 0.6 mm.yr^{-1} to nearly 0 mm.yr^{-1} as a consequence of diffusion over the initial flat topography. After that time and until the first 1 Myr, the mean denudation rate increases but remains lower than the uplift rate, leading to the increase in average elevation over this time period. ~~Next in~~In the following ~~0.5~~1 Myr, E_{av} exceeds the uplift rate to reach up to ~~1.03~~0.104 mm.yr^{-1}~~. It then~~ before it gently decreases to 0.1 mm.yr^{-1} ~~during~~until the ~~rest~~end of the simulation. This shows that topography tends to - but never reaches - a strict steady state over the simulation time. Abrupt changes in E_{av} after ca. ~~2 Myr, 2.5 Myr and 3.2 Myr can also be highlighted (Fig. 3b). These brief variations~~2.5, 3.5, 4.5 and 9.5 Myr (red circles in Figure 4b) are related to major local captures in the drainage network, which can be observed during the model evolution (red circles in Fig. ~~2d~~3e and f and Supplementary Video n°1).

~~On the basis of~~Based on these results, we will consider that ~~quasi-~~a regional topographic steady-state is reached between 1.5 and 2 Ma, when the plateau relict topography is totally eroded and E_{av} begins to decrease (Figs. ~~2~~3 and ~~3~~4). This time is consistent with the time required to reach topographic steady state proposed from models with constant uplift rate and no horizontal advection (Willett et al., 2001).

3.2 Basin-wide denudation rates variability

We calculate basin-wide denudation rates E upstream of each stable drainage network confluence after 2.5 Myr, 5 Myr and 10 Myr of simulation (Figs. ~~4a, b and c). As explained in the method section, we compiled the results obtained for five runs using the same parameters as the reference model, in order to increase the number of sampled basins.~~5a, b and c,

Mis en forme: Anglais(États Unis)

Mis en forme: Anglais(États Unis)

Mis en forme: Anglais(États Unis)

Mis en forme: Anglais(États Unis)

Mis en forme: Anglais(États Unis)

Mis en forme: Anglais(États Unis)

Mis en forme: Anglais(États Unis)

Mis en forme: Anglais(États Unis)

respectively). Regardless of the duration, we observe a significant variability in the calculated denudation rates depending on basin size. ~~This~~As exposed by Forte & Whipple (2018), the erosion rate contrasts across divides is spatially limited to areas very near the divides. Thus, the variability is maximum for small basins (ca. 1 km²) and decreases with increasing basin area. In our approach, small basins are nested in larger ones. Hence, these results can be related to the averaging of denudation rates along the drainage network, in agreement with the measurements of Matmon et al. (2003b). This variability also decreases with time (Figs. ~~4a, b and~~ 5a-c). For basins with an excess of denudation relative to the uplift rate U, the E/U ratio can reach up to ~~3~~2.5 after 2.5 Myr but only 2 after 5 Myr and 1.~~5~~7 after 10 Myr. Basins with a denudation excess that stand out of the general trend at 10 Ma (Fig. 5c) are associated with a capture event visible in figure 4b. For basins with a deficit of denudation, ~~this~~the evolution of the ratio is less obvious. It can be lower than 0.~~25~~5 after 2.5 Myr, but increases slightly to 0.~~4 after 5~~6 until 10 Myr. These results reflect a significant spatial variability of the difference between basin-wide denudation rates and ~~0.5 after 10 Myr~~uplift rate. To assess more accurately the temporal evolution of this variability, we calculate $\bar{E}$ every 0.5 Myr for three distinct categories of basin sizes: 1-2 km^2, 10-20 km^2 and 100-200 km^2. We then estimate the mean absolute deviation (MAD) from the uplift rate by considering separately basins with a denudation in excess or in deficit (Fig. ~~4d~~5d). Until 1.5 Ma, basins are located on the plateau where denudation rate is null. This leads to a low MAD for basins with a denudation deficit and to the absence of basins with a denudation excess. After 1.5 Ma, basins in deficit exhibit an ~~asymptotic~~ increase in MAD from nearly -0.~~2~~15 to -0.~~05~~04 mm.yr^{-1}, regardless of the area class considered. For basins in excess, the MAD value decreases through time, depending on drainage area : from ca. 0.~~28 mm.yr^{-1}~~25 to ca. 0.~~05~~07 mm.yr^{-1} for basins with an area of 1-2 km~~² and 10-20 km²;~~², from ca. 0.~~14~~2 mm.yr^{-1} to ca. 0.~~05~~07 mm.yr^{-1} for basins ~~with an area~~ of ~~100-200km². These results reflect a significant spatial variability of~~ 10-20 km² and from ca. 0.7 to ca. 0.04 mm.yr^{-1} for the ~~difference between basin-wide denudation rates and uplift rate in our reference models.~~largest basins. We ~~also~~ see a coherent evolution of this difference over the simulation time, consistent with the model progression toward ~~a total~~ topographic equilibrium.

The spatial variability of the denudation rates is neither homogeneous nor randomly distributed (Fig. ~~5a~~6a). The location of drainage basins with denudation rates far from the equilibrium value of 0.1 mm.yr^{-1} coincides with migrating drainage divides (Fig. ~~2e~~3d) and with cross-divide contrasts in ~~headwater~~channel χ, ~~slope~~gradient and ~~elevation~~height (Figs. ~~5b, c and~~ 6b-d). Following Willett et al. (2014) and Forte and Whipple (2018), the divide migrations predicted by these contrasts are consistent with the direction of divide mobility obtained from our model. One may note that the higher the contrast in these parameters across the divide, the higher the deviation of the denudation rate from the uplift rate, and therefore from topographic equilibrium. ~~These~~None of sampled basin in this data-set contains a knickpoint. Thus, these results based on simulations assuming uniform and constant properties as well as constant boundary conditions confirm that the dispersion observed in denudation rates is primarily controlled by divide migration. Basins that expand (shrink) show higher (lower) denudation rates compared to uplift rate, and are hereafter referred to as aggressors (victims), following the terminology adopted by Willett et al. (2014).

Mis en forme: Anglais(Royaume-Uni)

Mis en forme: Anglais(Royaume-Uni)

Mis en forme: Anglais(États Unis)

Mis en forme: Anglais(États Unis)

Mis en forme: Anglais(États Unis)

Mis en forme: Anglais(États Unis)

Mis en forme: Anglais(États Unis)

Mis en forme: Anglais(États Unis)

Mis en forme: Anglais(États Unis)

3.3 Deviation of denudation rates from the uplift rate, and basin aggressivity

Willett et al. (2014) showed that the basin-averaged cross-divide contrast in χ, could be used to deduce an aggressivity metric for basins. We extend this basin-scale approach to the Gilbert's metrics recently proposed by Forte and Whipple (2018) including cross-divide contrast in headwater ~~slope and elevation. Hereinafter, we refer to these aggressivity metrics based on cross-divide contrast in headwater χ, headwater slope (gradient) and headwater elevation (height) as $\Delta\chi$, ΔG and ΔH,~~gradient and elevation.~~respectively.~~

We here assess the relationship between the E/U ratio and these aggressivity metrics. First, to exclude variability related to both basin area and time, we focus on a single class of basins with a size of ~~10-20~~2-4 km² gathered from five computed reference models after a simulation duration of 2.5 Myr. Denudation rates may be affected by knickpoints, which are a source of transient perturbation at the scale of the catchment. Therefore, in order to focus only on perturbations associated with drainage divide dynamics, basins that contain knickpoints are ignored. In agreement with cross-divide metrics tested by Forte and Whipple (2018), ~~aggressor~~graphs in figure 7 must be divided into four quadrants. Aggressor (victim) basins have negative (positive) ~~$\Delta\chi$~~$\Delta\chi_{av}$ and ~~ΔH~~ΔH_{av} values and conversely positive (negative) ~~ΔG~~ΔG_{av} value~~.~~ (Fig. 2). Theoretically, aggressor (victim) basins have higher (lower) denudation rates than the underlying uplift rate. ~~Therefore graphs in figure 6 must be divided into four quadrants, with aggressors situated in the lower-left one, and victims in the higher-right one.~~ This result is verified for ca. ~~91, 88~~81 %, 52 % and ~~82~~81 % of basins for ~~aggressivity metric based on headwater χ, slope and elevation values,~~$\Delta\chi_{av}$, ΔG_{av} and ΔH_{av}, respectively~~ (Figs. 6a, b and c). Several basins depart significantly from the expected quadrants for ΔG and ΔH: these exhibit significant knickpoints in their drainage network that increase measured denudation rates.~~. For this limited dataset, the evolution between E/U and both ~~$\Delta\chi$~~$\Delta\chi_{av}$ and ~~ΔG can~~ΔH_{av} may be defined by a linear relationship (~~Figs. 6a and b). Part of the dispersion observed around this first-order trend may be explained by approximations in the calculation of denudation rates and aggressivity metrics.~~Fig. 7b). Compared to other metrics, ~~ΔH seems to be~~ΔG_{av} is less sensitive to drainage migration and shows a more scattered distribution ~~(Fig. 6c)~~.

In natural settings, the stage of evolution of landscapes cannot be easily defined and the total amount of basins with a specific size may be limited. The large dataset ~~provided by~~from our ~~model~~modeling can provide further insights by gathering the results obtained every 0.5 Myr for seven classes of basin areas expanding geometrically with a multiplying factor of 2 from 1-2 to 64-128 km² (Figs. ~~6d, e and f). Denudation rates can be affected by knickpoints, which are an additional source of transient perturbation at the scale of the catchment. Therefore, in order to focus on perturbations associated with drainage divide dynamics, basins that contain knickpoints are ignored.~~ 7b). Basins that contain knickpoints are discarded from the analysis.~~Our results highlight the major control of basin size on the dispersion E/U.~~ When all classes of drainage areas are combined together, we still obtain a clear relationship between aggressivity metrics and E/U, with 77 %, 56 % and 78 % of basins lying in aggressors or victims quadrants for $\Delta\chi_{av}$, ΔG_{av} and ΔH_{av}, respectively (Fig 7b). Our results highlight the major control of basin size on the dispersion E/U.~~$\Delta\chi$ and ΔG and E/U (Fig 6d and e). One may note however~~ Part of the variability intrinsic for each class of basin area may in turn be explained by heterogeneities in aggressivity between different

Mis en forme: Anglais(États Unis)
Mis en forme: Anglais(États Unis)
Mis en forme: Anglais(États Unis)
Mis en forme: Anglais(États Unis)
Mis en forme: Anglais(États Unis)
Mis en forme: Anglais(États Unis)
Mis en forme: Anglais(États Unis)
Mis en forme: Anglais(États Unis)
Mis en forme: Anglais(États Unis)

parts of a basin. Figure 7c shows that this dispersion is related to the standard deviation of aggressivity metrics, $\Delta\chi_{std}$, ΔG_{std} and ΔH_{std}. In other words, basins where different divide segments migrate at different rates or in different directions are more scattered. The lower the confidence index, the more scattered the results (Fig. 7d). Thus, some dispersion may come from approximations due to undocumented divide segments performed when averaging metrics differences between reference basins (Fig. 2). One may note two different trends for victim and aggressor basins. Aggressors show a more scattered distribution for ~~$\Delta\chi$~~$\Delta\chi_{av}$ and ~~ΔG~~ΔG_{av} metrics. When compared to victims, these basins have hillslopes closer to the critical value Sc (Fig. S3). Hence, the dispersion may be explained by the non-linear relationship existing between denudation rates and basin slope (Montgomery and Brandon, 2002; Binnie et al., 2015).~~ Therefore, a simple linear trend is no longer sufficient to properly fit our results. Hence we consider victim and aggressor basins independently assuming two linear trends between E/U and each aggressivity metric.~~

4 Discussion

4.1 Sensitivity tests

The reference model involves various parameters related to uplift, fluvial incision and hillslope denudation~~ and fluvial incision.~~. A systematic analysis of ~~all parameters~~ trade-off between allparameters is out of the scope of this manuscript. ~~Here, we do not investigate the effect of erodibility, because it remains poorly constrained in nature and because our study is mostly focused on channel head properties.~~ In this section, we assess the sensitivity of the results to both tectonic and ~~hillslope~~erosion processes, by studying the specific impact of uplift U, erodibility K, diffusivity D and critical hillslope gradient Sc taken separately. Varying these parameters may change the simulation time required to erode the plateau associated with the initial boundary conditions. In this section, to reduce sensitivity dependence on these initial conditions, we only considerresults obtained between 5 Ma and 10 Ma.

4.1.1 Sensitivity to uplift rate

We ~~vary the tectonic~~test rock uplift ~~rate from~~rates of 0.~~5~~01 mm.yr^{-1}, 0.1 mm.yr^{-1} (hereafter called reference model) and 1 mm.yr^{-1} to ~~2 mm.yr^{-1}, which is in~~cover the range ~~observed in moderately active mountain belts; e.g. the Alborz, the Alps or the Caucasus~~of a large variety of geodynamic settings (Champagnac et al., ~~2009; Djamour et al., 2010; Vincent et al., 2011).~~2012). It is well~~-~~ known that a river responds to a fall in base level (due to changes in rock uplift rate or other forcing) by cutting downward into its bed, deepening and widening its active channel. In our simulations, changes in uplift rate lead to variations in the ~~geometry~~density of the drainage network. Compared to the reference model, an uplift rate of ~~2~~1 mm.yr^{-1} (0.~~5~~01 mm.yr^{-1}) results in ~~an~~ a decrease (increase~~ (decrease~~) of ~~river channelization – inversely proportional to~~ drainage density~~ – which induces larger (smaller) river basins, a lower (higher) range of values for $\Delta\chi$ and ΔG and a higher (lower) range of values for ΔH (Fig. 7). More importantly, our simulations suggest a linear~~. These results are consistent with

Mis en forme: Anglais(États Unis)

Mis en forme: Anglais(États Unis)

Mis en forme: Anglais(États Unis)

Mis en forme: Anglais(États Unis)

Mis en forme: Exposant

previous studies that show an inverse relationship between ~~tectonic uplift~~drainage density and ~~denudation~~erosion rates~~. As a result, assuming no climate-tectonic feedback we obtain no significant changes~~ in equilibrium topography when using a threshold slope for diffusion processes (Tucker and Bras, 1998; Clubb et al., 2016). An increase in uplift rate favors river entrenchment leading to increase the range of ΔG_{av} and ΔH_{av} (Fig. 8). ~~relationship between the calculated aggressivity~~Hence, these two Gilbert's metrics ~~and the E/U ratio for~~appear to be well suited to diagnose local disequilibrium for higher uplift rates ~~ranging between 0.5~~(i.e. ≥ 1 mm.yr^{-1} ~~and 2 mm.yr^{-1}.~~). Conversely increase uplift rate induces a lower range of values for $\Delta\chi_{av}$. This last observation is explained by the decrease of drainage density, and associated stream length.

Maximum variability of E/U reaches a factor regardless the assumed uplift rate between 1 mm.yr^{-1} and 0.01 mm.yr^{-1}. The observed small differences suggest that limited uplift rate promote diffusive processes (see Sect. 4.1.3).

4.1.2 Influence of erodibility

Fluvial erosion is proportional to the erodibility coefficient K that may reflect, among others, rock strength and climate. We let this parameter vary between 5.10^{-6} m$^{(1-2m)}$.yr^{-1} and 5.10^{-5} m$^{(1-2m)}$.yr^{-1}. As expected from (Eq.1 and 3), we find that erodibility and uplift rates have opposite effects. Lower (higher) values of erodibility lead to higher (lower) average topography. Thus, an increase (decrease) in erodibility decreases (increases) the range of all aggressivity metrics (Fig. 9). Lower values of erodibility also increase the range of the E/U ratio. Models with higher (lower) erodibility reach a quasi-topographic steady state earlier (at a later stage). Hence, differences in the variability of E/U may be related to different stages of evolution for each models over the period we consider (5 to 10 Ma) (Fig. 5d).

4.1.3 Influence of hillslope processes

Hillslope denudation is proportional to the diffusivity coefficient D and depends on the critical slope ~~Sc~~Sc (Eq. 2). To test the effect of hillslope processes, we ~~first vary~~let D vary between 10^{-3} ~~and 10^{-1}~~ m^2.yr^{-1}~~. We find~~ and 10^{-1} m^2.yr^{-1}. Compared to the reference model, we find no ~~major difference with the reference model over that range of values for D (Fig.~~ differences in the case of a lower diffusivity (i.e. 0.001 m².yr^{-1}) (Fig. 10c). In contrast, for models with higher diffusivity coefficient (i.e. 0.1 m².yr^{-1}), this parameter has a significant effect on both the range of E/U and the aggressivity metric ΔG_{av} (Fig. 10a). This result derives from a stronger impact of diffusive processes in the upstream parts of the drainage network, consistent with the observations described in section 4.1.1.~~8).~~ ~~Denudation intensity also varies inversely to the square of the critical hillslope gradient Sc (Eq. 2).~~ Assuming a critical slope between 20° and 40°, we find that Sc ~~is a parameter influencing aggressivity metrics (Fig. 9). As in the case of variations in uplift rate, changes in Sc lead to differences in the organization of the drainage network. Compared to the reference model, a low Sc leads to large river channelization, reducing the range of all aggressivity metrics, but~~ does not affect significantly the relationship between the E/U ratio and the studied metrics~~.~~

Mis en forme: Anglais(États Unis)

Mis en forme: Anglais(États Unis)

Mis en forme: Anglais(États Unis)

Mis en forme: Anglais(États Unis)

Mis en forme: Anglais(États Unis)

~~These observations are consistent with a landscape where hillslopes are completely determined by the assumed critical slope value.~~ (Fig.11).

Altogether, these sensitivity tests demonstrate the robustness of our findings~~: $\Delta\chi$ and ΔG~~. Regardless of the tested parameter values, we observe a relationship between aggressivity metrics and deviation of denudation rates from uplift rates. Thus, aggressivity metrics are, to the first-order, reliable metrics to assess the effect of divide mobility on basin-wide denudation rates inferred from simulations. In the following section, we apply this approach to field observations and discuss the consequences for sampling and interpretation.

4.2 ~~Implication~~Implications for the interpretation of basin-wide denudation ~~rate interpretation~~rates

Over the last decades, measurements of cosmogenic radionuclides (CRN) concentration in alluvial sediments (see Granger et al., 2013 and references therein), of suspended sediments (Gabet et al., 2008) and of detrital thermochronology (Huntington and Hodges, 2006) have become common practices to assess basin-wide denudation rates. However, their interpretation remains debated, even in settings where topographic steady state is supposedly achieved regionally.

4.2.1 Application to the Great Smoky Mountains

As previously mentioned (Matmon et al., 2003a, b), while the Great Smoky Mountains in the southern Appalachians are expected to be in a quasi-topographic steady state, basin-wide denudation rates show a strong dispersion up to a factor of ~~2~~two in comparison ~~with~~to the estimated uplift rate (~~0.025 to~~ca. 0.03 mm.yr^{-1}, see Fig. 1). ~~Basins in~~We use the ~~Great Smoky Mountains exhibit average slope values ranging between 20 and 30° (Matmon et al., 2003a). This may suggest that hillslopes are close to the critical angle of repose. On the basis of these assumptions, we consider that our approach is applicable to the~~data associated with 40 basins ~~studied~~originally sampled by Matmon et al~~.~~., (2003a, b~~), even though estimated uplift rates differ by nearly two orders of magnitude when compared to the uplift rates used in our models. We use the data associated with 40 basins originally sampled by Matmon et al., (2003a~~) and for which denudation rates were re-calculated by Portenga and Bierman (2011). Following our method, we calculate the three basin-averaged aggressivity metrics ~~$\Delta\chi$, ΔG~~ $\Delta\chi_{av}$, ΔG_{av} and ~~ΔH~~ ΔH_{av} associated with these 40 catchments (Fig. ~~10~~12; See also Fig. ~~S4~~S3). The calculation of χ requires to define the elevation of the catchment outlets H_b and the m/n ratio (Eq. 4). As underlined by Forte and Whipple (2018), the choice of the "correct" outlet elevation is non-trivial in natural settings. We first consider a local base level given by the Tennessee ~~river~~River. To test the relevance of this choice, we also ~~test~~use a base level located at a fixed arbitrary elevation H_b= 400 m. We ~~use~~assume the same m/n ratio value of 0.45 as used ~~in the~~by Willett et al. (2014)~~ study~~ for the Great Smoky Mountains. For all calculated metrics, the majority (ca. ~~75~~58% for ~~ΔG~~ ΔG_{av} and ~~55~~ca. 66% for ~~ΔH)~~ ΔH_{av}) of the basins are located in the expected quadrants~~.~~ (see Fig. 7). However, more attention must be given to the results based on ~~$\Delta\chi$.~~ $\Delta\chi_{av}$. For this metric, ~~~62~~ca. 58% of the analyzed basins lie in the expected quadrant when we consider the Tennessee river as the local base level

Mis en forme: Anglais(États Unis)
Mis en forme: Anglais(États Unis)
Mis en forme: Anglais(États Unis)
Mis en forme: Anglais(États Unis)
Mis en forme: Anglais(États Unis)
Mis en forme: Anglais(États Unis)
Mis en forme: Anglais(États Unis)
Mis en forme: Anglais(États Unis)
Mis en forme: Anglais(États Unis)

versus ~~~67~~ca. 68% for H_b= 400 m (Fig. ~~10). If~~12b). Although the ~~general result remains~~overall results are similar ~~here~~, we show that the choice of a different base level H_b leads to significant variations in ~~$\Delta\chi$~~$\Delta\chi_{av}$ for individual basins. This highlights the main weakness of the ~~$\Delta\chi$~~$\Delta\chi_{av}$ metric, which is highly sensitive to the choice of the proper base level H_b. Nevertheless, our results confirm the findings of Willett et al. (2014), suggesting that a significant part of the data variance observed in the Matmon et al. (2003a, b) can be explained by divide migration (Fig. ~~10~~12), raising this possible explanation for the variability of most natural data~~-~~-sets. One may note that the Southern Appalachians exhibit migrating knickpoints that can locally affect denudation rates (Gallen et al., 2011~~-~~; Gallen et al., 2013). This last point can also explain part of the observed variability in this dataset but this specific impact is beyond the scope of the present ~~manuscript~~study.

Based on both our simulations and this field dataset, we propose to favor the use of ~~the Gilbert metric ΔG based on the cross-divide contrast in channel head local slope (Forte~~ $\Delta\chi_{av}$ and ~~Whipple, 2018).~~ ΔH_{av}. Among the tested metrics, ~~ΔH~~ΔG_{av} appears the least sensitive to disequilibrium, ~~and $\Delta\chi$ requires better constraining and defining objective criteria for H_b.~~excepted in active mountain belts with rock uplift U ≥ 1 mm.yr^{-1}.

4.3.2 Assessment of topographic disequilibrium

Topographic steady-state is a very convenient assumption and concept to deduce the uplift pattern in mountains ranges from denudation rates, and thus to obtain significant information on the geometry of active structures and on orogen dynamics (Lavé and Avouac, 2001, Godard et al., 2014 ; Scherler et al., 2014; Le Roux-Mallouf et al., 2015). However, this assumption is seldom verified at the scale of sampled watersheds.

On the basis of our modeling, we show that the competition between low-order basins has a significant impact on basin-wide denudation rates. The proposed approach provides a new tool to assess the potential ~~maximum~~ deviation from topographic steady state based on aggressivity metrics and drainage area, which can both be inferred from a simple DEM~~. The~~: the closer to zero the aggressivity metrics and the lower the standard deviation of cross-divide metrics, the more representative ~~to~~of uplift rate ~~are~~ the measured denudation rates. ~~However it still remains dispersion of denudation rates values, especially for smaller catchments.~~

~~Based on our sensitivity tests for moderately active orogens (with uplift rates between 0.5 and 2 mm/yr), the empirical relationship between ΔG and E/U obtained from the reference model (Fig. 6) can be used to assess the topographic disequilibrium of basins. Especially for victim basins ($\Delta G < 0$), this relationship exhibits a linear relationship:~~

$$\cancel{\frac{E-U}{U} = 0.03\Delta G \quad \text{for basin area} > 50\ \text{km}^2,} \qquad \cancel{(6)}$$

Mis en forme: Anglais(États Unis)

Mis en forme: Anglais(États Unis)

Mis en forme: Anglais(États Unis)

~~For the sake of simplicity our models involve spatially homogenous and time invariant parameters. Additional simulations are now needed to test this approach in more complex settings, including spatial and temporal variability in climate and tectonic forcing or internal landscape parameters like erodibility.~~

4.4.3 Improvement of sampling strategy

Basin-wide denudation rates obtained from CRN concentration measurements, suspended sediments or detrital thermochronology depend on many parameters including lithology, ice cover, rainfall, landslide activity or tectonic uplift (Vance et al., 2003; Bierman and Nichols, 2004; Wittmann et al., 2007; Yanites et al., 2009; Norton et al., 2010; Godard et al., 2012; Whipp and Elhers, 2019). Hence, to unravel the influence of tectonics from other processes, a specific sampling strategy is usually recommended: (1) to sample catchments with homogeneous lithologies to limit the effect of spatial variations in the abundance of target minerals in bedrock formations; (2) to select catchments with no ice cover (past or present) because the input of glacier-derived sediments can significantly complicate the interpretation of CRN concentrations; (3) to choose areas with spatially uniform rainfall distribution; and (4) to consider watersheds where the relative contribution of landslides to long-term landscape evolution is low. Unfortunately, these different criteria imply to select watersheds with variable sizes. The first three criteria favor the sampling of small catchments, whereas the last one requires basins large enough to be less affected by landslides.~~ Indeed, Niemi et al. (2005) proposed that mixing effects efficiently dampen the stochastic nature of hillslope sediment delivery by landsliding above a critical catchment area. Considering an uplift rate of 0.5-2 mm.yr^{-1}, the recommended minimum area needed to mitigate these biases associated with the stochastic input from landslides is of 50 to 200 km^2.~~

Our approach suggests the need to pre-assess targeted basins for their potential divide mobility before sampling for CRN concentration measurements. If the objective is to quantify the background uplift rate, one should sample basins that satisfy the conditions we previously enounced in the current section and also display an aggressivity close to zero and with the smallest associated standard deviation. Conversely, to quantify the specific denudation rate associated with the migration of drainage divides, small aggressor or victim basins should be favored.

Based on our simulations, a relationship between the maximum of erosion variability (0.5 and 99.5 percentiles, respectively) due to divide mobility $[(E-U)/U]_{max}$ and the catchment size A can be derived (Fig. ~~11~~13). Our results suggest a logarithm dependence between these two parameters, regardless of the assumed U, K, D and S_c~~.~~:

$$[(E-U)/U]_{max} = c_1 \log(A) + c_2 \quad \text{for} \quad 1\ \text{km}^2 < A < 100\ \text{km}^2 , \tag{7}$$

~~For victim basins ($\Delta G < 0$), c_1 ~ 0.05 and c_2 ~ −0.5, whereas for aggressor basins c_1 ~ −0.14 and c_2 ~ 1. This provides a new additional guideline for the design of sampling strategies in terms of basin size. For instance, considering a quasi-steady state mountain belt with an uplift rate of 1 mm.yr^{-1}, the minimum basin area required for an erosion rate variability~~

Mis en forme: Anglais(États Unis)
Mis en forme: Anglais(États Unis)
Mis en forme: Anglais(États Unis)
Mis en forme: Anglais(États Unis)
Mis en forme: Anglais(États Unis)
Mis en forme: Anglais(États Unis)
Mis en forme: Anglais(États Unis)
Mis en forme: Anglais(États Unis)
Mis en forme: Anglais(États Unis)
Mis en forme: Anglais(États Unis)
Mis en forme: Anglais(États Unis)
Mis en forme: Anglais(États Unis)
Mis en forme: Anglais(États Unis)

~~lower than 0.5 mm.yr^{-1} is ca. 1 km^2 for victim basins and 30-40 km^2 for aggressor basins.~~with c_1 and c_2 two parameters that depend on balance between erosion processes, uplift rate and state of evolution of the landscape.

5 Conclusions

Calculations from a Landscape Evolution Model assuming spatially uniform uplift, rock strength and rainfall confirm that the concept of topographic steady state is relevant at the scale of entire mountain belts, but represents an oversimplification at the scale of individual watersheds. Our simulations underline the role of divide mobility on deviations from equilibrium, which can lead to significant differences between tectonic uplift rate and basin-wide denudation rates even if an overall topographic steady state is achieved at large scale.

To better assess these deviations, we propose new basin-averaged aggressivity metrics - $\Delta\chi_{av}$, ΔG_{av} and ΔH_{av} - based on the approach of Willett et al. (2014) and Forte and Whipple (2018). They include mean cross-divide contrasts in channel~~ heads~~ χ, local ~~slope~~gradient and ~~elevation at the scale of entire river basins.~~height. From our calculations, ~~contrasts in channel-head elevation appear~~$\Delta\chi_{av}$ is the most reliable aggressivity metric to ~~be weakly sensitive to~~ assess local disequilibrium~~, whereas,~~ but is highly depend on the ~~basin denudation to~~ chosen base level, which remains hard to constrain. Gilbert's metrics ΔG_{av} and ΔH_{av} are more suitable for relatively high uplift ~~ratio E/U exhibits a nonlinear relationship with $\Delta\chi$ and ΔG. Together, these two~~rate (i.e. ≥ 1 mm.yr-1). Altogether, our metrics reveal that ~~E/U~~deviation of denudation rates from uplift rate related to divide migrations depends on both basin aggressivity and basin area. This last parameter has a key control on the dispersion in E/U, which can reach a factor of two, regardless of the imposed uplift rate (here 0.~~5-2 mm.~~01-1 mm.yr^{-1}), erodibility (here 5.10^{-6}-5.10^{-5} m$^{(1-2m)}$.yr^{-1}), diffusivity (here 10^{-3}-10^{-1} m^2.yr^{-1}) and hillslope gradient (here 20°-40°). By comparing our results to CRN measurements from the Great Smoky Mountains (Matmon, 2003a, b), we show that this approach can be used to improve field sampling strategies and provides a new tool to derive a minimal uncertainty in basin-wide denudation rates due to topographic disequilibrium.

For the sake of simplicity our models involve spatially homogenous and time invariant parameters. Additional simulations are now needed to test this approach in more complex settings, including spatial and temporal variability in climate and tectonic forcing or parameters like stream power equation exponents n and m.

Acknowledgments

We are greatly indebted to referees Fiona Clubb and Adam Forte for providing constructive reviews that significantly improve the quality of the manuscript. We thank Wolfgang Schwanghart and Benjamin Campforts for providing the TopoToolBox and TTLEM codes to analyze and to simulate landscape evolution. Timothée Sassolas-Serrayet's Ph.D. is supported by a fellowship from the French Ministry for Higher Education. ~~We thank Wolfgang Schwanghart and Benjamin Campforts for providing the programme TopoToolBox and TTLEM to analyze and to simulate landscape evolution.~~ We

Mis en forme: Anglais(Royaume-Uni)

Mis en forme: Anglais(Royaume-Uni)

Mis en forme: Anglais(Royaume-Uni)

Mis en forme: Anglais(Royaume-Uni)

Mis en forme: Anglais(Royaume-Uni)

Mis en forme: Anglais(Royaume-Uni)

Mis en forme: Anglais(Royaume-Uni)

Mis en forme: Anglais(Royaume-Uni)

Mis en forme: Anglais(Royaume-Uni)

Mis en forme: Anglais(Royaume-Uni)

Mis en forme: Anglais(Royaume-Uni)

Mis en forme: Anglais(Royaume-Uni)

Mis en forme: Anglais(États Unis)

Mis en forme: Anglais(États Unis)

acknowledge funding of the French Agence National de la Recherche, grant ANR-18-CE01-0017 (Topo-Extreme). ~~This~~Through the work of Martine Simoes, this study contributes to the IdEx Université de Paris ANR-18-IDEX-0001~~. This~~, and is IPGP contribution # XXX~~.~~.

References

Binnie, S. A., Phillips, W. M., Summerfield, M. A., and Fifield, L. K.: Tectonic uplift, threshold hillslopes, and denudation rates in a developing mountain range. Geology 35(8), 743-746, 2007.

Bierman, P., and Nichols, K.K.: Rock to sediment slope to sea with 10 Be rates of landscape change. Annual Review of Earth and Planetary Sciences 32, 215-255, 2004.

Blöthe, J. H., Korup, O., and Schwanghart, W.: Large landslides lie low: Excess topography in the Himalaya-Karakoram ranges, Geology, 43, 523–526, doi:10.1130/G36527.1, 2015.

Burbank, D. W., Leland, J., Fielding, E., Anderson, R. S., Brozovic, N., Reid, M. R., and Duncan, C.: Bedrock incision, rock uplift and threshold hillslopes in the northwestern Himalayas. Nature 379(6565), 505, 1996.

Champagnac, J.D., ~~Schlunegger, F., Norton, K., von Blanckenburg, F., Abbühl, L.M. and Schwab, M.: Erosion-driven uplift of the modern Central Alps. Tectonophysics 474(1-2), 236-249, 2009.~~Molnar, P., Sue, C., Herman, F.: Tectonics, climate and mountain topography. Journal of geophysical research, 117, B02403, doi:10.1029/2011JB008348, 2012.

Campforts, B., and Govers, G.: Keeping the edge: A numerical method that avoids knickpoint smearing when solving the stream power law. Journal of Geophysical Research: Earth Surface, 120(7), 1189-1205, 2015.

Campforts, B., Schwanghart, W., and Govers, G.: Accurate simulation of transient landscape evolution by eliminating numerical diffusion: the TTLEM 1.0 model. Earth Surface Dynamics 5, 47-66, 2017.

~~Djamour, Y., Vernant, P., Bayer, R., Nankali, H.R., Ritz, J.F., Hinderer, J., Hatam, Y., Luck, B., Le Moigne, N., Sedighi, M. and Khorrami, F.: GPS and gravity constraints on continental deformation in the Alborz mountain range, Iran. Geophysical Journal International 183(3), 1287-1301, 2010.~~

Clubb, F. J., Mudd S. M., Attal M., Milodowski D. T., and GrieveS. W. D.: The relationship between drainage density, erosion rate, and hilltop curvature: Implications for sediment transport processes, J. Geophys. Res. Earth Surf., 121, 1724-1745, doi:10.1002/2015JF003747, 2016.

Culling, W. E. H.: Soil Creep and the Development of HillsideSlopes, J. Geol., 71, 127–161, doi:10.1086/626891, 1963.

Dahlquist, M.P., West, A.J., & Li, G.: Landslide-driven drainage divide migration. Geology, 46(5), 403–406. doi:10.1130/g39916.1, 2018.

England, P. and Molnar, P.: Surface uplift, uplift of rocks, and exhumation of rocks. Geology 18, 1173-1177, 1990.

Forte, A.M. and Whipple, K.X.: Criteria and tools for determining drainage divide stability. Earth and Planetary Science Letters 493, 102-117, 2018.

Mis en forme: Police :+Titres (Times New Roman)

Mis en forme: Police :+Titres (Times New Roman)

Mis en forme: Police :+Titres (Times New Roman)

Mis en forme: Police :+Titres (Times New Roman)

~~Gallet~~Gallen, S.F., Wegmann, K.W., Frankel, K.L., Hughes, S., Lewis, R.Q., Lyons, N., Paris, P., Ross, K., Bauer, J.B., and Witt, A.C.: Hillslope response to knickpoint migration in the Southern Appalachians: implications for the evolution of post-orogenic landscapes. Earth Surface Processes Landforms 36, 1254-1267, 2011.

~~Gallet~~Gallen, S. F., Wegmann, K. W., and Bohnenstiehl, D.R.: Miocene rejuvenation of topographic relief in the southern Appalachians. GSA Today 23, no.2, 2013.

Gabet, E. J., Burbank, D. W., Pratt-Sitaula, B., Putkonen, J., and Bookhagen, B.: Modern erosion rates in the High Himalayas of Nepal. Earth and Planetary Science Letters 267(3–4), 482–494, ~~-~~https://doi.org/10.1016/j.epsl.2007.11.059, 2008.

Gilbert GK.: Report on the Geology of the Henry Mountains. USGS Report, Government Printing Office, Washington, D.C., 1877.

Godard, V., Lavé, J., and Cattin, R.: Numerical modelling of erosion processes in the Himalayas of Nepal: Effects of spatial variations of rock strength and precipitation. Geological Society, London, Special Publications 253(1), 341-358, 2006.

Godard, V., Burbank, D.W., Bourlès, D.L., Bookhagen, B., Braucher, R. and Fisher, G.B.: Impact of glacial erosion on 10Be concentrations in fluvial sediments of the Marsyandi catchment, central Nepal. Journal of Geophysical Research: Earth Surface 117(F3), 2012.

Godard, V., Bourlès, D.L., Spinabella, F., Burbank, D.W., Bookhagen, B., Fisher, G.B., Moulin, A. and Léanni, L.: Dominance of tectonics over climate in Himalayan denudation. Geology 42(3), 243-246, 2014.

Granger, D.E., Lifton, N.A., and Willenbring, J.K.: A cosmic trip: 25 years of cosmogenic nuclides in geology. GSA Bulletin 125(9-10), 1379-1402, 2013.

Harel, M.-A., Mudd, S.M. and Attal, M.: Global analysis of the stream power law parameters based on worldwide ^{10}Be denudation rates. Geomorphology 268, 184-196, https://doi.org/10.1016/j.geomorph.2016.05.035, 2016.

Hasbargen, L.E. and Paola, C.: Landscape instability in an experimental drainage basin. Geology 28, 1067-1070, 2000.

Hasbargen, L.E. and Paola, C.: How predictable is local erosion rates in eroding landscapes? Prediction in Geomorphology 135, 231-240, https://doi.org/10.1029/135GM16, 2003.

Huntington, K. W., and Hodges, K. V.: A comparative study of detrital mineral and bedrock age-elevation methods for estimating erosion rates. Journal of Geophysical Research: Earth Surface 111(3), 1–11, https://doi.org/10.1029/2005JF000454, 2006.

Jungers, M.C., Bierman, P.R., Matmon, A., Nichols, K., Larsen, J. and Finkel, R.: Tracing hillslope sediment production and transport with in situ and meteoric 10Be. Journal of Geophysical Research: Earth Surface 114, F04020, https://doi.org/10.1029/2008JF001086, 2009.

Hack JT.: Interpretation of erosional topography in humid temperate regions. American Journal of Science 258-A, 80-97, 1960.

Kirby, E., and Whipple, K.: Quantifying differential rock-uplift rates via stream profile analysis. Geology 29(5), 415-418, 2001.

Lavé, J., and Avouac, J.P.: Fluvial incision and tectonic uplift across the Himalayas of central Nepal. Journal of Geophysical Research 106(B11), 26,561-26,591, 2001.

Le Roux-Mallouf, R., Godard, V., Cattin, R., Ferry, M., Gyeltshen, J., Ritz, J.F., Drupka, D., Guillou, V., Arnold, M., Aumaître, G. and Bourles, D.L.: Evidence for a wide and gently dipping Main Himalayan Thrust in western Bhutan. Geophysical Research Letters 42(9), 3257-3265, 2015.

Matmon, A., Bierman, P.R., Larsen, J., Southworth, S. Pavich, M., Kinkel, R., and Caffee, M.: Erosion of an ancient mountain range, the Great Smoky Mountains, North Carolina and Tennessee. American Journal of Science 303, 817-855, 2003a.

Matmon, A., Bierman, P.R., Larsen, J., Southworth, S. Pavich, M., Caffee, M.: Temporally and spatially uniform rates of erosion in the southern Appalachian Great Smoky Mountains. Geology 31, 155-158, 2003b.

Miller, S.R., Sak, P.B., Kirby, E., and Bierman, P.R.: Neogene rejuvenation of central Appalachian topography: Evidence for differencial rock uplift from stream profiles and erosion rates. Earth and Planetary Science Letters 369-370, 1-12, https://doi.org/10.1016/j.epsl.2013.04.007, 2013.

~~Montgomery, D. R., and Foufoula-Georgiou, E.: Channel network source representation using digital elevation models. Water Resources Research 29(12), 3925-3934, 1993.~~

Montgomery, D.R.: Slope distributions, threshold hillslopes, and steady-state topography. American Journal of science 301(4-5), 432-454, 2001.

Montgomery, D. R., and Brandon, M. T.: Topographic controls on erosion rates in tectonically active mountain ranges. Earth and Planetary Science Letters 201(3-4), 481-489, 2002.

~~Niemi, N.A., Oskin, M., Burbank, D.W., Heimsath, A.M. and Gabet, E.J.: Effects of bedrock landslides on cosmogenically determined erosion rates. Earth and Planetary Science Letters 237(3-4), 480-498, 2005.~~

Norton, K.P., von Blanckenburg, F., and Kubik, P.W.: Cosmogenic nuclide-derived rates of diffusive and episodic erosion in the glacially sculpted upper Rhone Valley, Swiss Alps, Earth Surf. Processes Landforms 35(6), 651–662, 2010.

Pelletier, J. D.: Persistent drainage migration in a numerical landscape evolution model. Geophysical Research Letters 31(20), L20501, 2004.

Pelletier, J. D.: Quantitative Modeling of Earth Surface Processes, Cambridge University Press, Cambridge, UK, 2008.

Perne, M., Covington, M.D., Thaler, E.A. and Myre, J.M.: Steady state, erosional continuity, and the topography of landscapes developed in layered rocks. Earth Surface Dynamics 5(1), 85-100, 2017.

Perron, J.T.: Numerical methods for nonlinear hillslope transport laws. Journal of Geophysical Research: Earth Surface 116, F02021, https://doi.org/10.1029/2010JF001801, 2011.

Perron, J. T., and Royden, L.: An integral approach to bedrock river profile analysis. Earth Surface Processes and Landforms 38, 570-576, 2012.

Portenga, E.W. and Bierman, P.R.: Understanding Earth's eroding surface with 10 Be. GSA today 21, 4-10, 2011.

Mis en forme: Police :+Titres (Times New Roman)

Mis en forme: Police :+Titres (Times New Roman)

Mis en forme: Police :+Titres (Times New Roman)

Mis en forme: Police :+Titres (Times New Roman)

Mis en forme: Police :+Titres (Times New Roman)

Mis en forme: Police :+Titres (Times New Roman)

Mis en forme: Police :+Titres (Times New Roman)

Mis en forme: Police :+Titres (Times New Roman)

Mis en forme: Police :+Titres (Times New Roman)

Mis en forme: Police :+Titres (Times New Roman)

Reiners, P. W., Ehlers, T. A., Mitchell, S. G., and Montgomery, D. R.: Coupled spatial variations in precipitation and long-term erosion rates across the Washington Cascades. Nature 426, 645-647, 2003.

Reinhardt, L. and Ellis, M.A.: The emergence of topographic steady state in a perpetually dynamic self-organized critical landscape. Water Resources Research 51, 4986-5003, 2015.

Richardson, P.W., Perron, J.T., and Schurr, N.D.: Influences of climate and life on hillslope sediment transport. Geology 47, 1–4, https://doi.org/10.1130/G45305.1, 2019.

Roering, J.J., Kirchner, J.W., and Dietrich, W.E.: Evidence for nonlinear, diffusive sediment transport on hillslopes and implications for landscape morphology. Water Resources Research 35, 853-870, 1999.

Royden, L., and Perron, J.T.: Solutions of the stream power equation and application to the evolution of river longitudinal profiles. Journal of Geophysical Research: Earth Surface 118(2), 497-518, 2013.

Scherler, D., Bookhagen, B. and Strecker, M.R.: Tectonic control on 10Be-derived erosion rates in the Garhwal Himalaya, India. Journal of Geophysical Research: Earth Surface 119(2), 83-105, 2014.

Schwanghart, W., and Scherler, D.: Short Communication: TopoToolbox 2 - MATLAB-based software for topographic analysis and modeling in Earth surface sciences. Earth Surface Dynamics 2, 1-7, 2014.

Stolar, D.B., Willett, S.D. and Montgomery, D.R.: Characterization of topographic steady state in Taiwan. Earth and Planetary Science Letters 261(3-4), 421-431, 2007.

Tucker, G.E., Bras, R.L. Hillslope processes, drainage density, and landscape morphology. Water Resources Reseach 34(10), 2751-2764, 1998.

Vance, D., Bickle M., Ivy-Ochs S., and Kubik P.W.: Erosion and exhumation in the Himalaya from cosmogenic isotope inventories of river sediment~~,~~. Earth Planet. Sci. Lett. 206(3–4), 273–288, 2003.

~~Vincent, S.J., Carter, A., Lavrishchev, V.A., Rice, S.P., Barabadze, T.G. and Hovius, N.: The exhumation of the western Greater Caucasus: a thermochronometric study. Geological Magazine 148(1), 1-21, 2011.~~

West, N., Kirby, E., Bierman, P., Slingerland, R., Ma, L., Rood, D. and Brantley, S. Regolith production and transport at the Susquehanna Shale Hills Critical Zone Observatory, part 2: insights from meteoric 10Be. Journal of Geophysical Research: Earth Surface 118(3), 1877-1896, 2013.

Whipp, D.M. and Elhers T.A.: Quantifying landslide frequency and sediment residence time in Nepal Himalaya. Sci. Adv. 5, eaav3482, 2019.

Whipple, K.X.: Fluvial landscape response time: How plausible is steady-state denudation?. American Journal of Science 301(4-5), 313-325, 2001.

Whipple, K.X., Forte, A.M., DiBiase, R.A., Gasparini, N.M. and Ouimet, W.B.: Timescales of landscape response to divide migration and drainage capture: Implications for the role of divide mobility in landscape evolution. Journal of Geophysical Research: Earth Surface 122(1), 248-273, 2017.

Willett, S.D., Slingerland, R. and Hovius, N.: Uplift, shortening, and steady state topography in active mountain belts. American journal of Science 301(4-5), 455-485, 2001.

Willett, S.D., McCoy, S.W., Perron, J.T., Goren, L. and Chen, C.Y.: Dynamic reorganization of river basins. Science, Science 343, 1248765, 2014.

Wittmann, H., von Blanckenburg, F., Kruesmann, T., Norton, K.P. and Kubik, P.W.: Relation between rock uplift and denudation from cosmogenic nuclides in river sediment in the Central Alps of Switzerland. Journal of Geophysical Research: Earth Surface 112, F04010, 2007.

Yanites, B.J., Tucker, G.E. and Anderson, R.S.: Numerical and analytical models of cosmogenic radionuclide dynamics in landslide-dominated drainage basins. Journal of Geophysical Research: Earth Surface 114, F01007, doi:10.1029/2008JF001088, 2009.

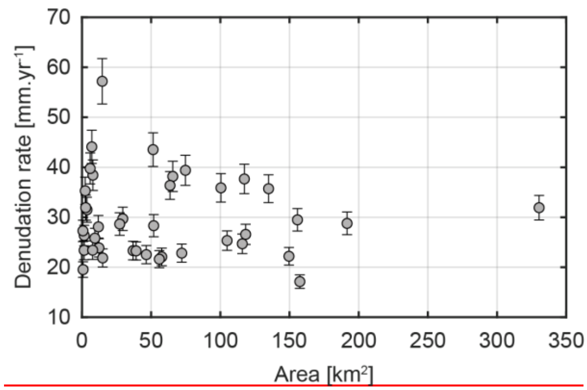

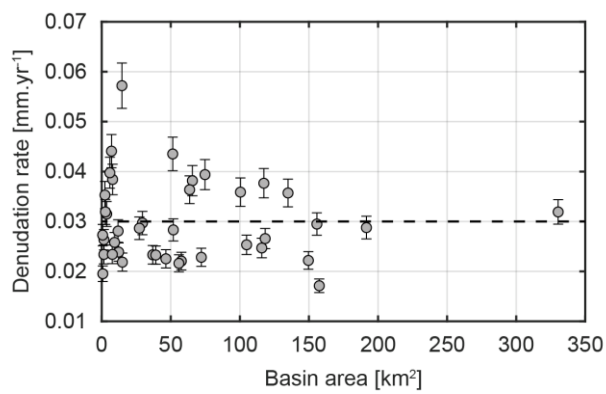

Figure 1: Basin-wide denudation rate variability as a function of drainage area in the Great Smoky Mountains. ~~Data originally~~Original dataset from Matmon et al~~., .~~ (2003a, b), denudation rates ~~are~~ reprocessed by Portenga and Bierman, (2011). Dashed black line show the estimated background uplift rate for the region of 0.03 mm.yr^{-1}.

Mis en forme: Anglais(Royaume-Uni)
Mis en forme: Anglais(Royaume-Uni)
Mis en forme: Anglais(Royaume-Uni)
Mis en forme: Anglais(Royaume-Uni)
Mis en forme: Anglais(Royaume-Uni)
Mis en forme: Anglais(Royaume-Uni)

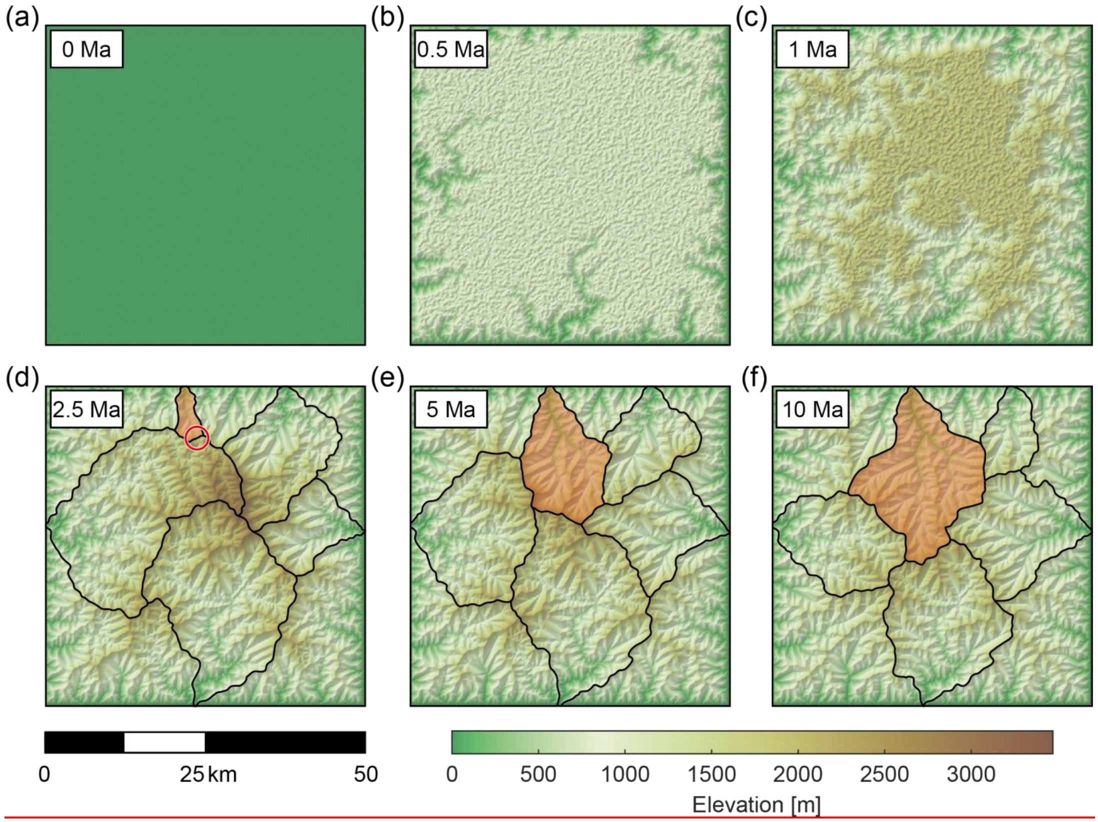
(a)
0 Ma
(b)
0.5 Ma
(c)
1 Ma
(d)
2.5 Ma
(e)
5 Ma
(f)
10 Ma
0
25 km
50
0
500
1000
1500
2000
2500
3000
Elevation [m]

640 ~~Figure 2~~

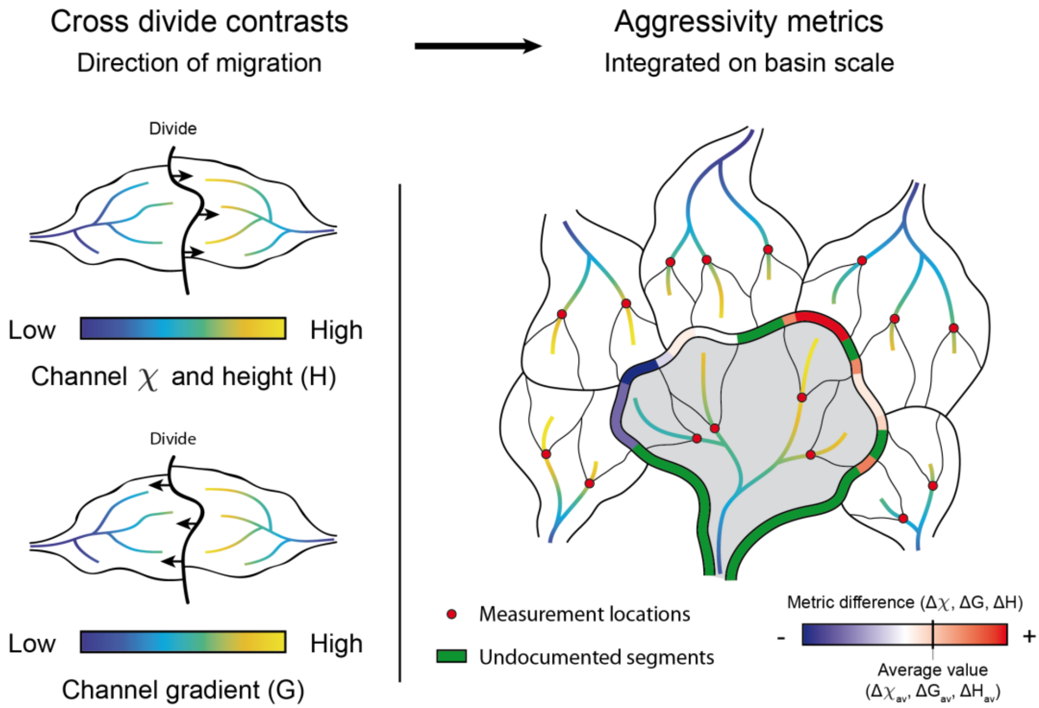

Figure 2: Conceptual relationship between cross-divide contrast in χ and Gilbert's metrics and divide migration as exposed by Willett et al. (2014) and Forte and Whipple, (2018). For χ and height, divides migrate toward the drainages that present higher values. For channel gradient, divides migrate toward the drainages that present lower values. In our study, channel χ, local gradient and height are measured at the outlet (indicated by red circles) of basins for a reference area (basins bounded with thin black lines). Aggressivity metrics are then calculated for a given basin (represented in grey) by averaging along its perimeter the individual across divide differences in metrics between reference basins. The proportion of perimeter which is not shared by two reference basins is measured to give a confidence index of the calculated aggressivity.

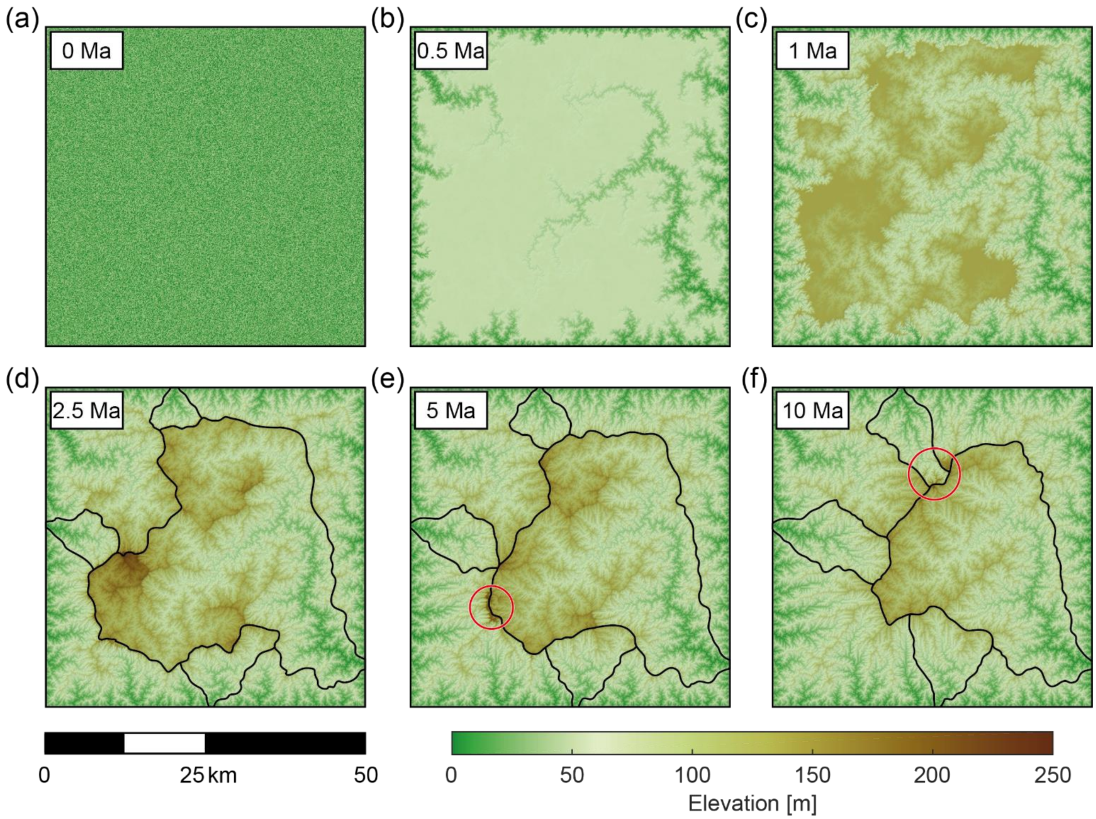

Figure 3: Map view of the temporal evolution of the reference model. Colorbar gives the model elevation. Black lines show the evolution - and the migration - over time of drainage divides for five drainage basins. ~~One basin is colored in orange to underline its expansion. The red circle~~Red circles in figure ~~3d shows the location of an imminent~~3e and 3f show transient topography associated with drainage capture after ~~2.~~5 and 10 Myr of simulation, respectively (see Supplementary Video n°1).

Mis en forme: Anglais(Royaume-Uni)
Mis en forme: Anglais(Royaume-Uni)
Mis en forme: Anglais(Royaume-Uni)
Mis en forme: Anglais(Royaume-Uni)
Mis en forme: Anglais(Royaume-Uni)
Mis en forme: Anglais(Royaume-Uni)
Mis en forme: Anglais(Royaume-Uni)

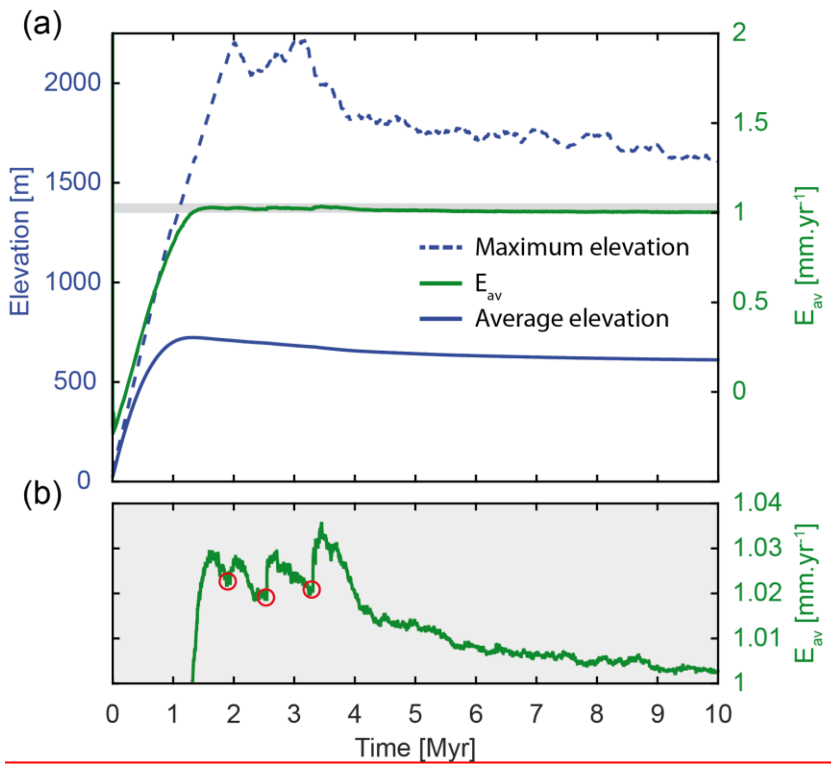
(a)
Maximum elevation
E_av
Average elevation
Elevation [m]
E_av [mm.yr^-1]
(b)
E_av [mm.yr^-1]
Time [Myr]

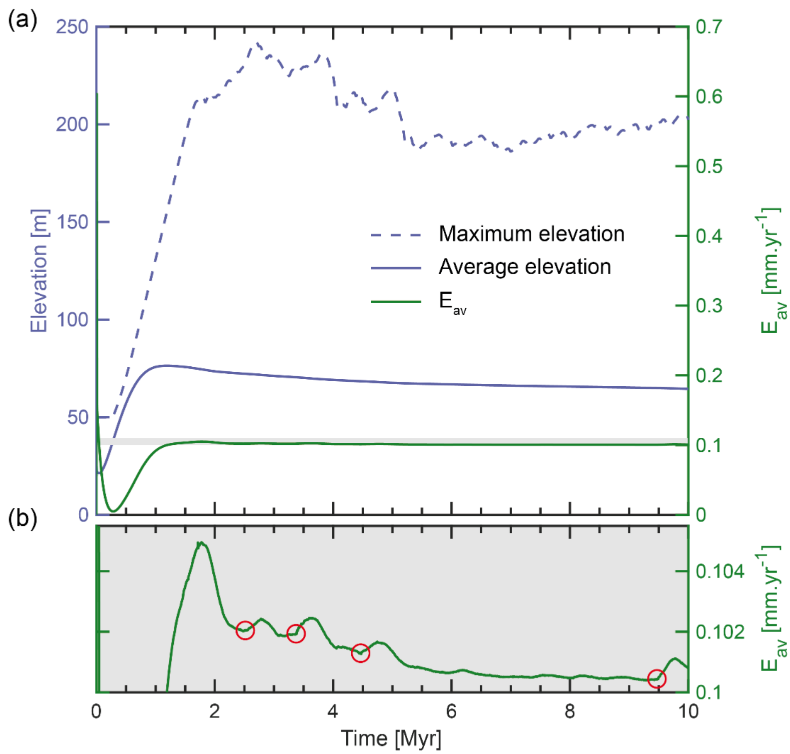

Figure ~~3~~4: Evolution of the reference model over time. (a) Average elevation (blue solid line), maximum elevation (blue dashed line) and average denudation rate (green solid line) over the whole model. (b) Expanded view of the mean denudation rate of figure ~~3a~~4a (in the light grey area). Red circles highlight significant stream captures that lead to an abrupt increase in average denudation rates over a subsequent period of several time steps~~.~~ (effects associated with stream captures at 4.5 Ma and 9.5 Ma are visible in Fig. 3e and 3f, respectively).

Mis en forme: Anglais(Royaume-Uni)

Mis en forme: Anglais(Royaume-Uni)

Mis en forme: Anglais(Royaume-Uni)

Mis en forme: Anglais(Royaume-Uni)

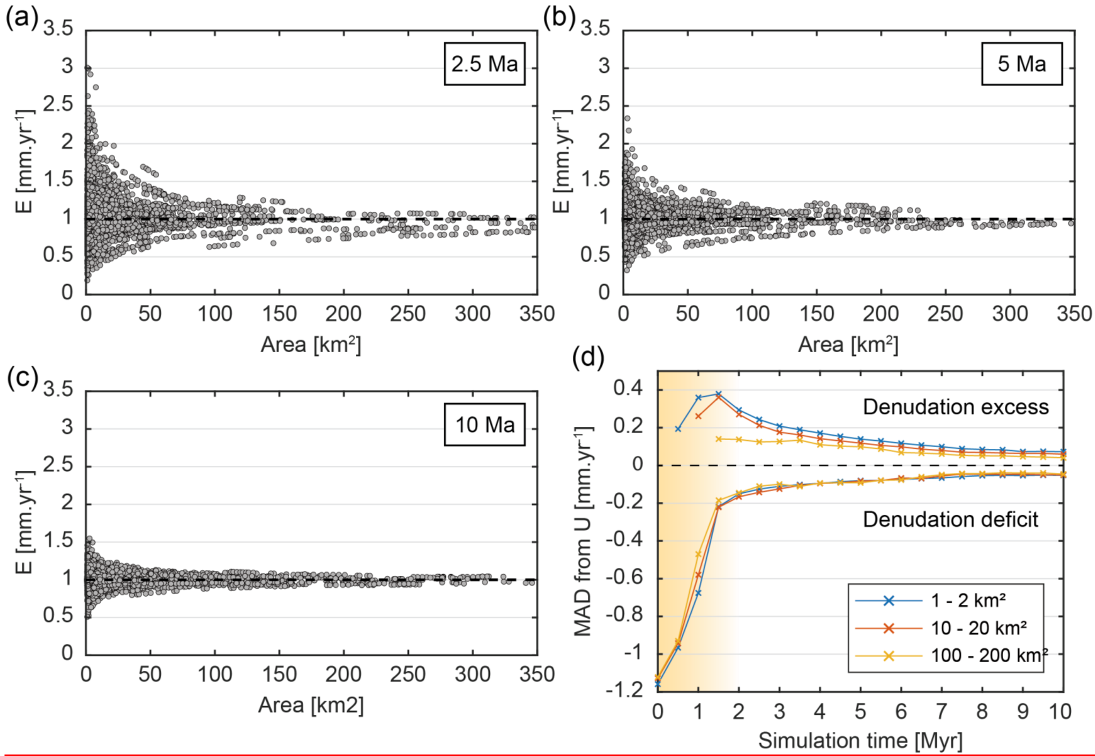
(a)
2.5 Ma
E [mm.yr-1]
Area [km2]
(b)
5 Ma
E [mm.yr-1]
Area [km2]
(c)
10 Ma
E [mm.yr-1]
Area [km2]
(d)
Denudation excess
Denudation deficit
MAD from U [mm.yr-1]
1 - 2 km²
10 - 20 km²
100 - 200 km²
Simulation time [Myr]

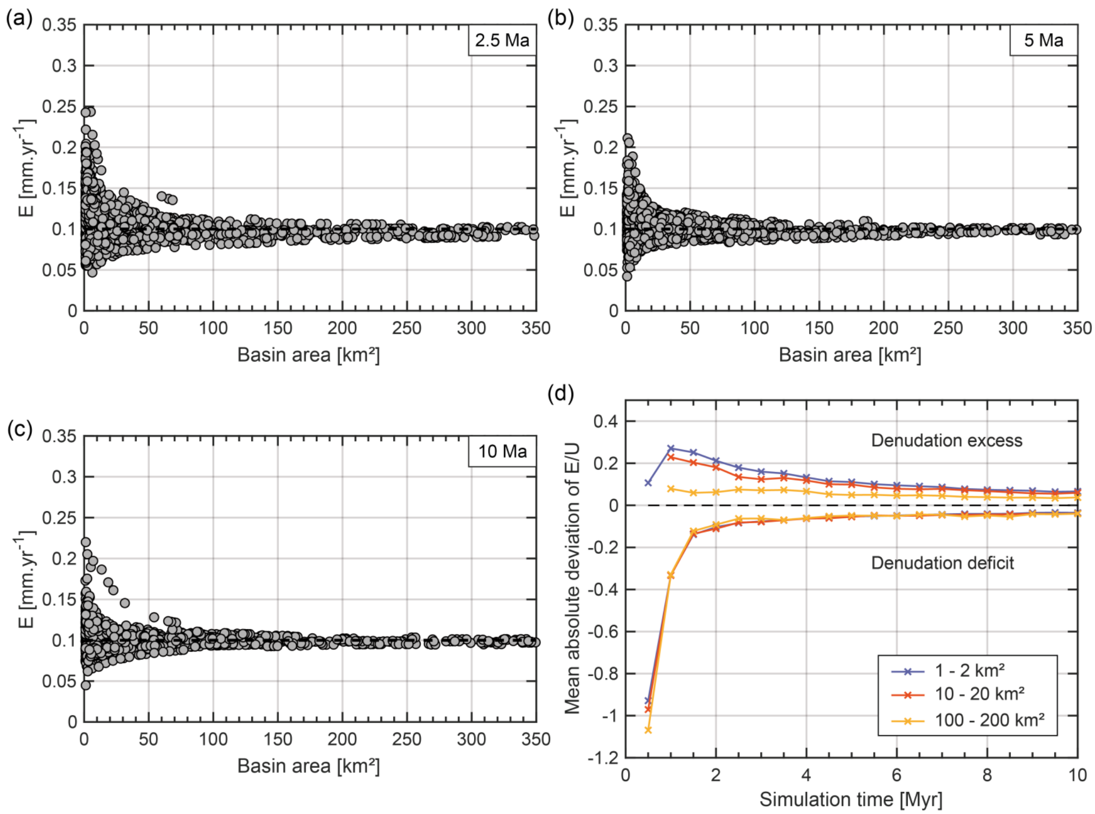

Figure ~~4~~5: Variability of denudation rates over time for a compilation of five simulations of the reference model~~.~~, with different initial noised DEM. (a) to (c) Variability of denudation rate as a function of basin area after 2.5, 5 and 10 Myr of simulation, respectively. (d) Mean absolute deviation (MAD) from uplift rate (0.1 mm.yr^{-1}) for three ~~sets~~classes of basin sizes: 1-2 km², 10-20 km² and 100-200 km²~~.~~ between 0.5 and 10 Ma. Negative (positive) deviation is related to ~~basins with a~~ deficit (excess) of denudation~~. The orange color gradient corresponds to the transient period associated with the rising plateau before the model reaches an average topographic equilibrium~~.

Mis en forme: Anglais(Royaume-Uni)
Mis en forme: Anglais(Royaume-Uni)
Mis en forme: Anglais(Royaume-Uni)
Mis en forme: Anglais(Royaume-Uni)
Mis en forme: Anglais(Royaume-Uni)
Mis en forme: Anglais(Royaume-Uni)
Mis en forme: Anglais(Royaume-Uni)
Mis en forme: Anglais(Royaume-Uni)

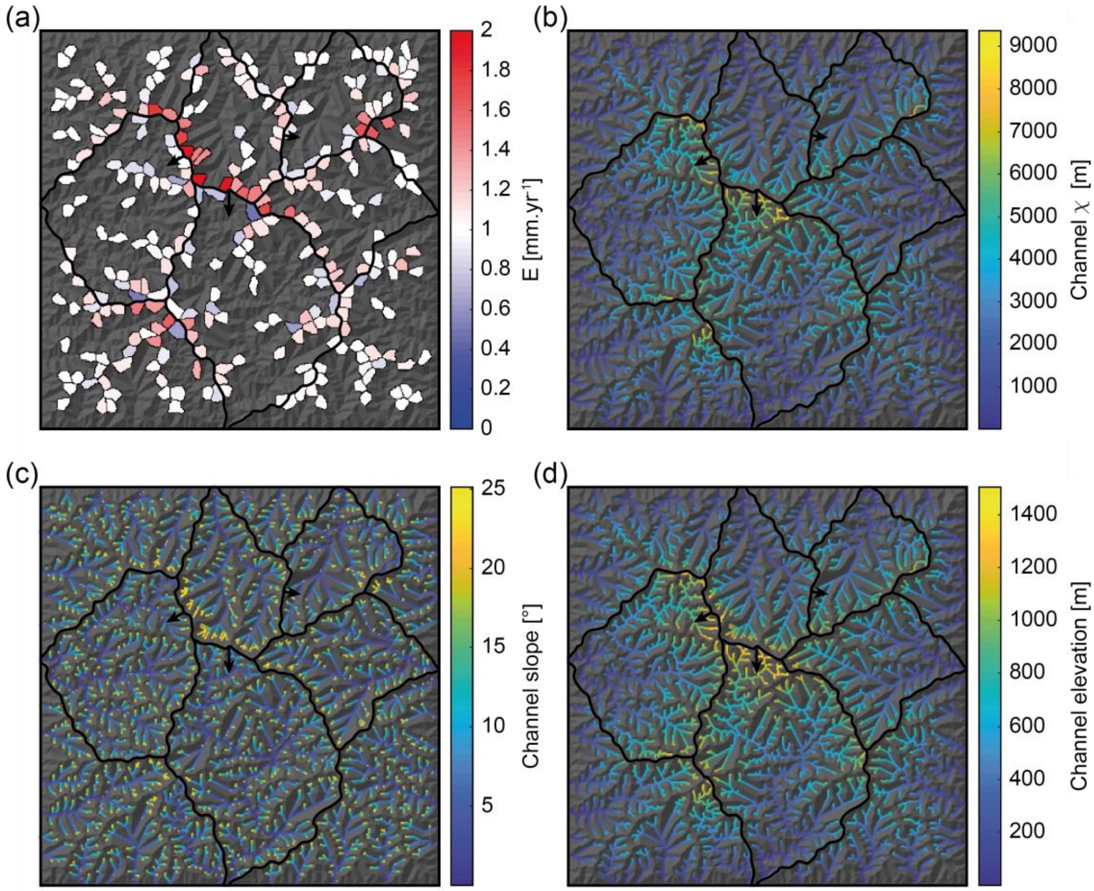
(a)
(b)
(c)
(d)
E [mm.yr-1]
2
1.8
1.6
1.4
1.2
1
0.8
0.6
0.4
0.2
0
Channel χ [m]
9000
8000
7000
6000
5000
4000
3000
2000
1000
Channel slope [°]
25
20
15
10
5
Channel elevation [m]
1400
1200
1000
800
600
400
200

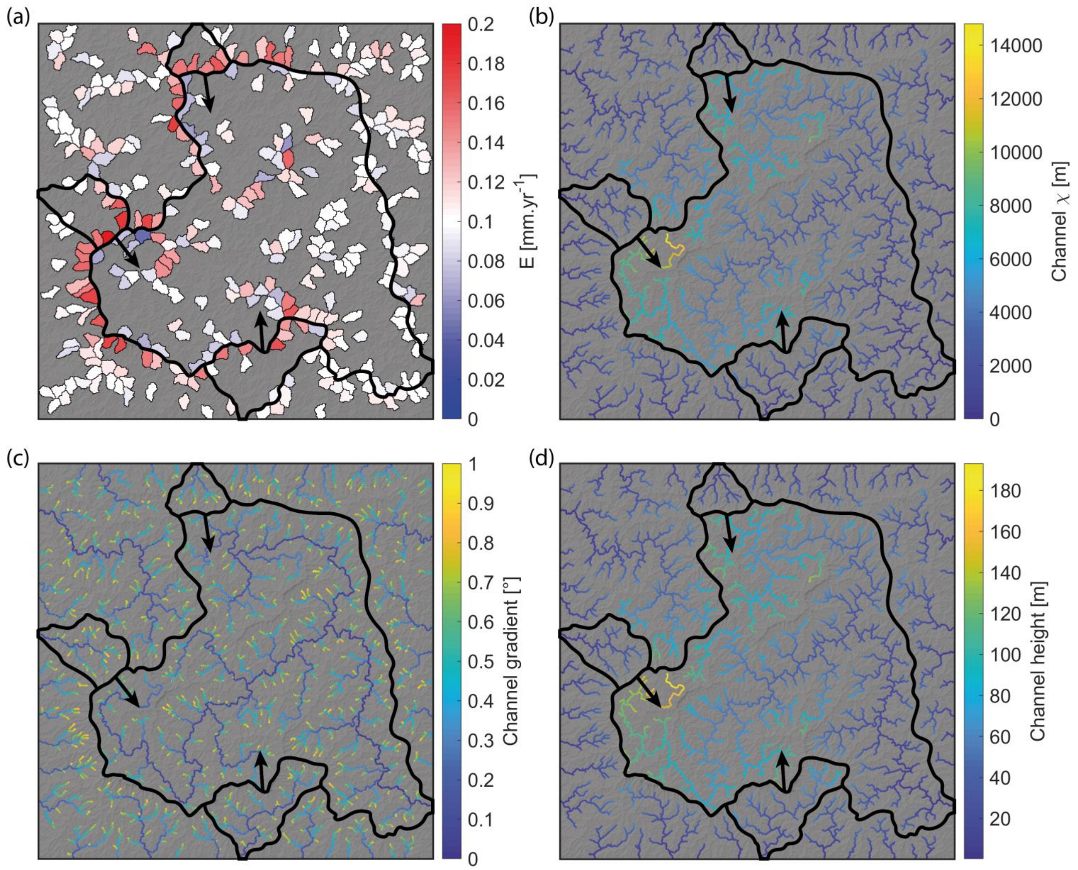

Figure ~~5~~6: Denudation rates and cross-divide contrast metrics obtained for the reference model after 2.5 Myr~~.~~ of simulation. Drainage network is extracted from a minimal drainage area of 1 km². (a) Map of denudation rates for basins of 2-4 km². Black thick lines correspond to basin divides in figure ~~2e~~2d. Black arrows, show the direction of divide migrations for ~~one basin.~~three selected basins. (b) χ map. (c) Channel ~~slope~~gradient map. (d) Channel ~~elevation~~height map.

Mis en forme: Anglais(États Unis)

Mis en forme: Police :Non Gras

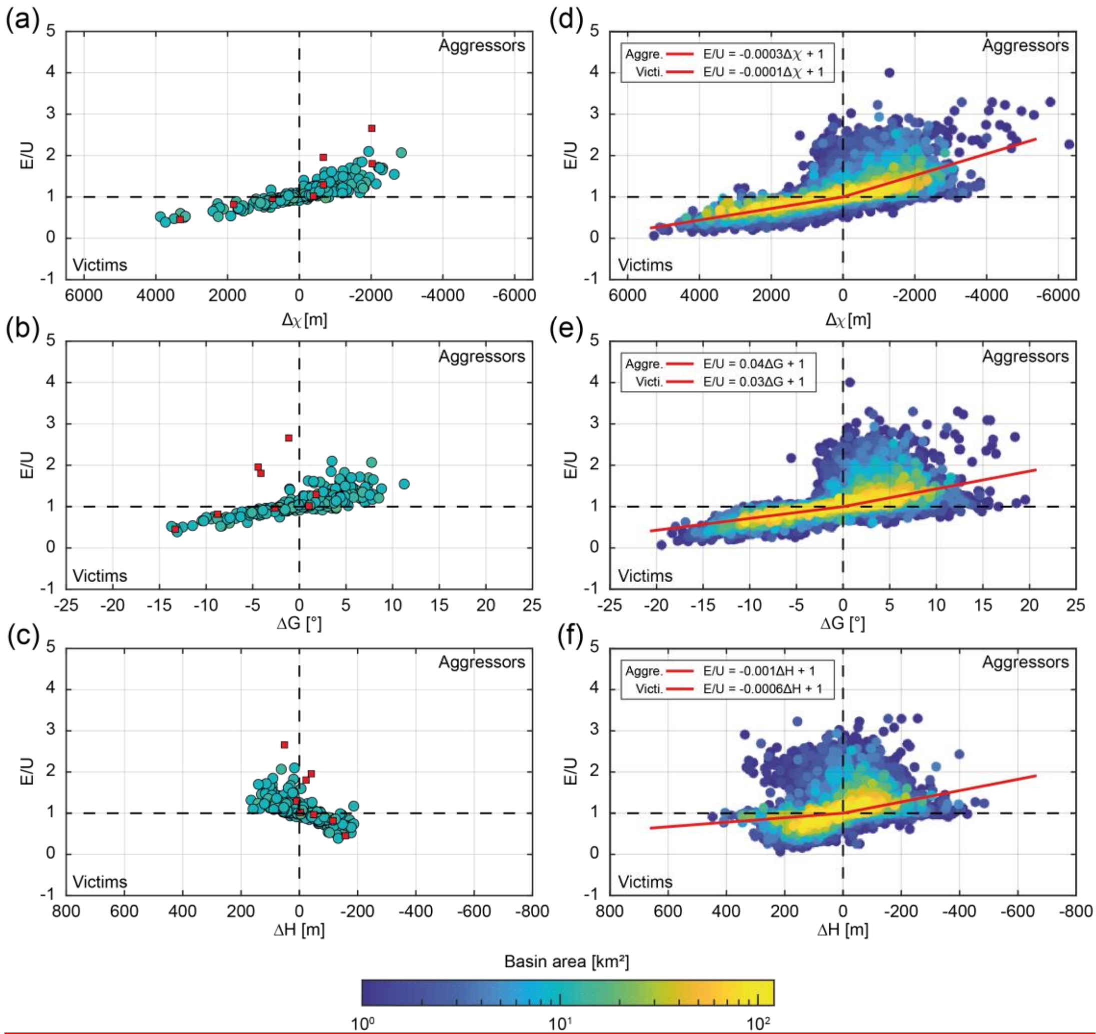
(a)
(b)
(c)
(d)
(e)
(f)
Aggressors
Victims
E/U
Δχ [m]
ΔG [°]
ΔH [m]
Aggre. E/U = -0.0003Δχ + 1
Victi. E/U = -0.0001Δχ + 1
Aggre. E/U = 0.04ΔG + 1
Victi. E/U = 0.03ΔG + 1
Aggre. E/U = -0.001ΔH + 1
Victi. E/U = -0.0006ΔH + 1
Basin area [km²]
10⁰
10¹
10²

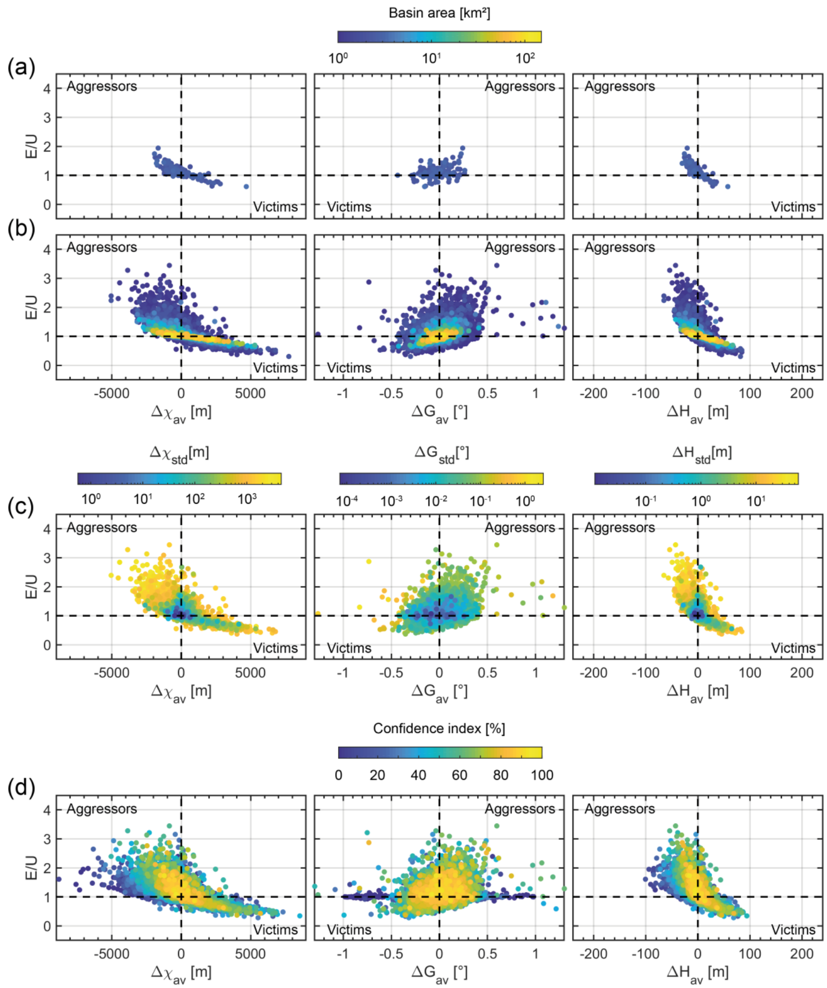

Figure ~~6~~7: Denudation rates normalized by uplift rate as a function of aggressivity metrics~~. Note that~~ and parameters influencing data dispersion. (a) Basins of 2-4 km² for the ~~x-axis is reversed for both $\Delta\chi$ and ΔH.~~reference model after 2.5 Myr of simulation. Color scale indicates basin area. ~~(a) to (c) Basins of 10-20 km² for reference model after 2.5 Myr. Red squares correspond to basins that contain at least one knickpoint. (d) to (f)~~ Basins with a confidence index lower than 50 % are discarded from the analysis. (b) Basins of variable sizes, ~~classified~~sorted in seven area classes expanding geometrically with a multiplying factor of 2 from 1-2 to 64-128 km², every 0.5 Myr over the time period 2-10 Myr. Color scale indicates basin area. ~~.5-10 Myr. Red lines are linear fits for victim and aggressor basins~~Basins with a confidence index lower than 50 % are discarded from the analysis. (c) Basin of 1-2 km² over the time period 2-10 Myr, color scale indicating the standard deviation of $\Delta\chi$, ΔG and ΔH, respectively. Basins with a confidence index lower than 50 % are discarded from the analysis. (d) Basin of 1-2 km² over the time period 2-10 Myr. Color scale indicates confidence index.

Mis en forme: Anglais(Royaume-Uni)
Mis en forme: Anglais(Royaume-Uni)
Mis en forme: Anglais(Royaume-Uni)
Mis en forme: Anglais(Royaume-Uni)
Mis en forme: Anglais(Royaume-Uni)
Mis en forme: Anglais(Royaume-Uni)
Mis en forme: Anglais(Royaume-Uni)
Mis en forme: Anglais(Royaume-Uni)
Mis en forme: Anglais(Royaume-Uni)
Mis en forme: Anglais(Royaume-Uni)
Mis en forme: Anglais(Royaume-Uni)
Mis en forme: Anglais(Royaume-Uni)

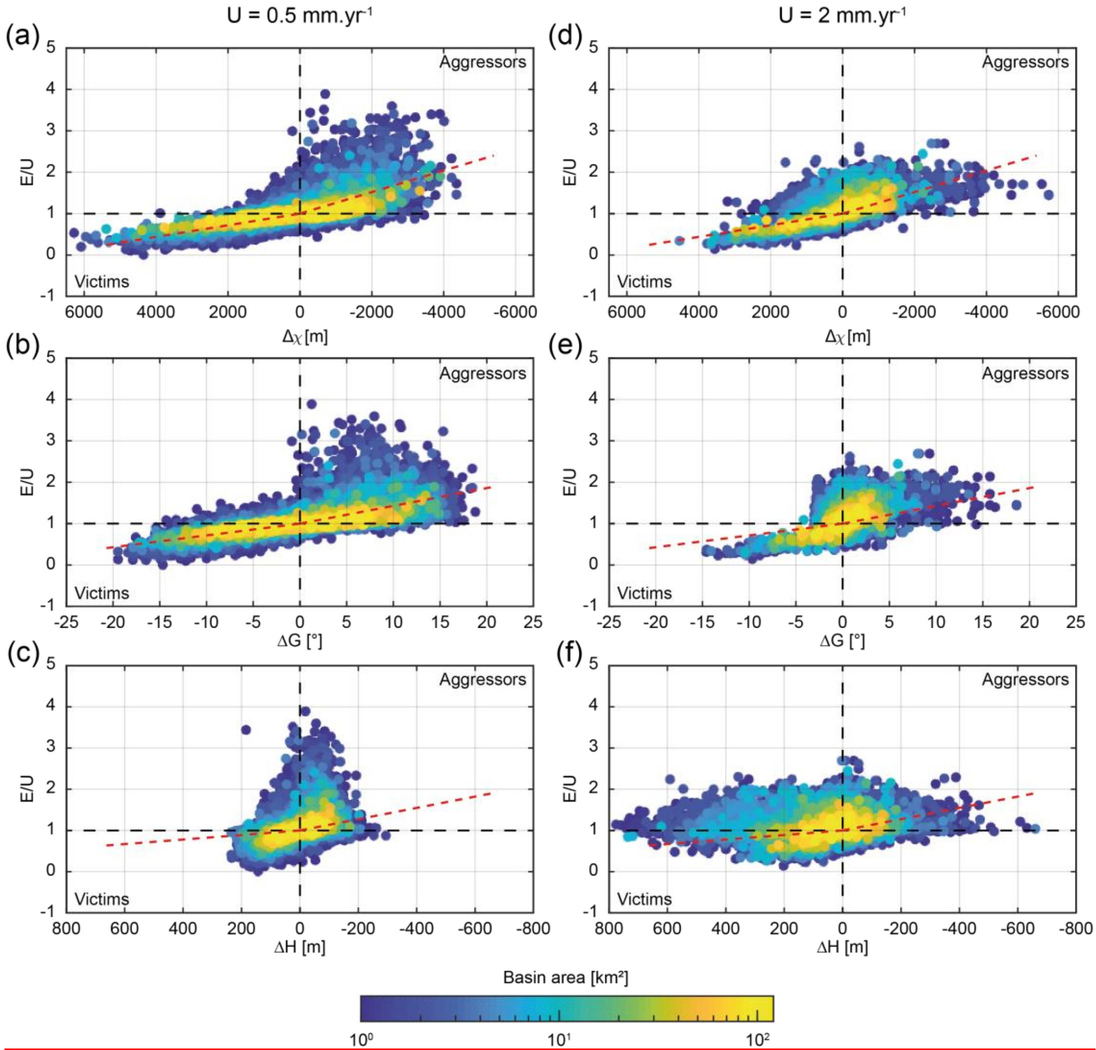
U = 0.5 mm.yr-1
U = 2 mm.yr-1
(a)
(b)
(c)
(d)
(e)
(f)
Aggressors
Victims
E/U
Δχ [m]
ΔG [°]
ΔH [m]
Basin area [km²]

705

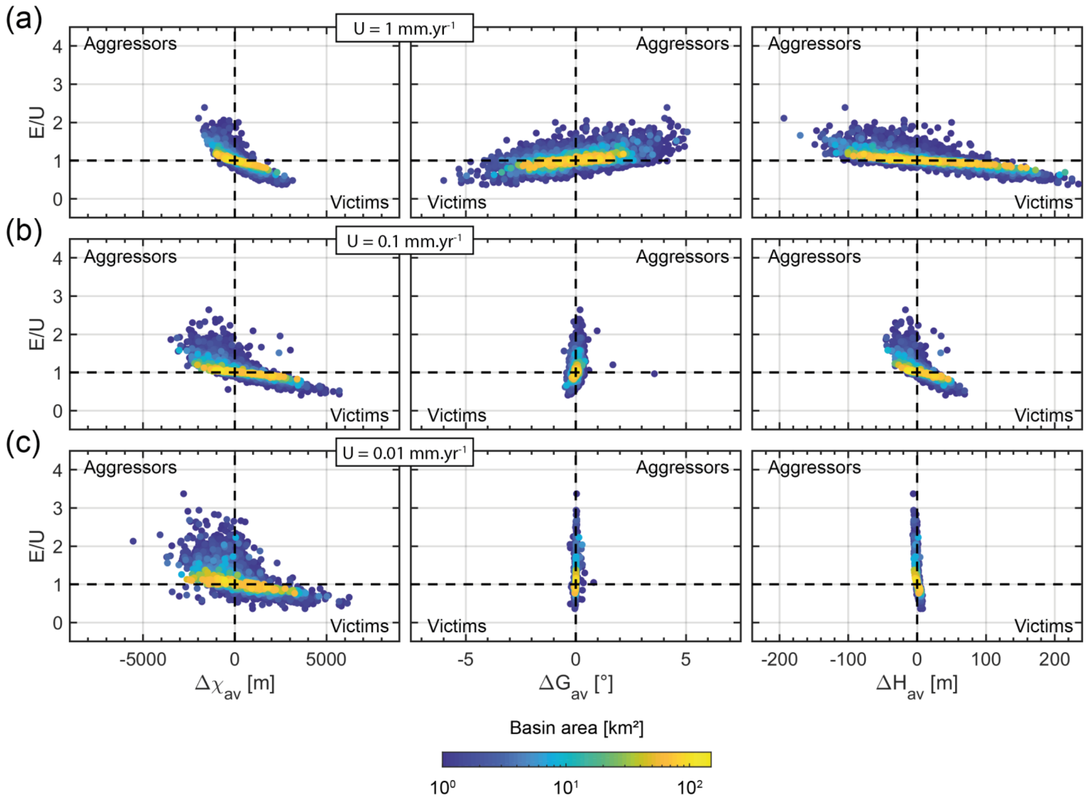

Figure ~~7~~8: Sensitivity to uplift rates. ~~Note that the horizontal axis is reversed for both $\Delta\chi$ and ΔH.~~ Color scale indicates basin area. Basins of variable sizes, sorted in seven area classes expanding geometrically with a multiplying factor of 2 from 1-2 to 64-128 km², every 0.5 Myr over the time period 5-10 Myr. Basins with a confidence index lower than 50 % are discarded from the analysis. (a) Results~~Color scale indicates basin area.~~ ~~Red dashed lines correspond to the linear fits obtained for the reference model (see figure 6). (a) to (c) Same as Fig. 6d-f,~~ with an uplift rate of ~~0.5~~1 mm.yr^{-1} ~~. (d) to (f) Same as Fig. 6d-f,~~. (b) Results with an uplift rate of ~~2 mm.yr^{-1}.~~ 0.1 mm.yr^{-1} (reference model). (c) Results with an uplift rate of 0.01 mm.yr^{-1}.

Mis en forme: Anglais(Royaume-Uni)
Mis en forme: Anglais(Royaume-Uni)
Mis en forme: Anglais(Royaume-Uni)
Mis en forme: Anglais(Royaume-Uni)
Mis en forme: Anglais(Royaume-Uni)
Mis en forme: Anglais(Royaume-Uni)
Mis en forme: Anglais(Royaume-Uni)

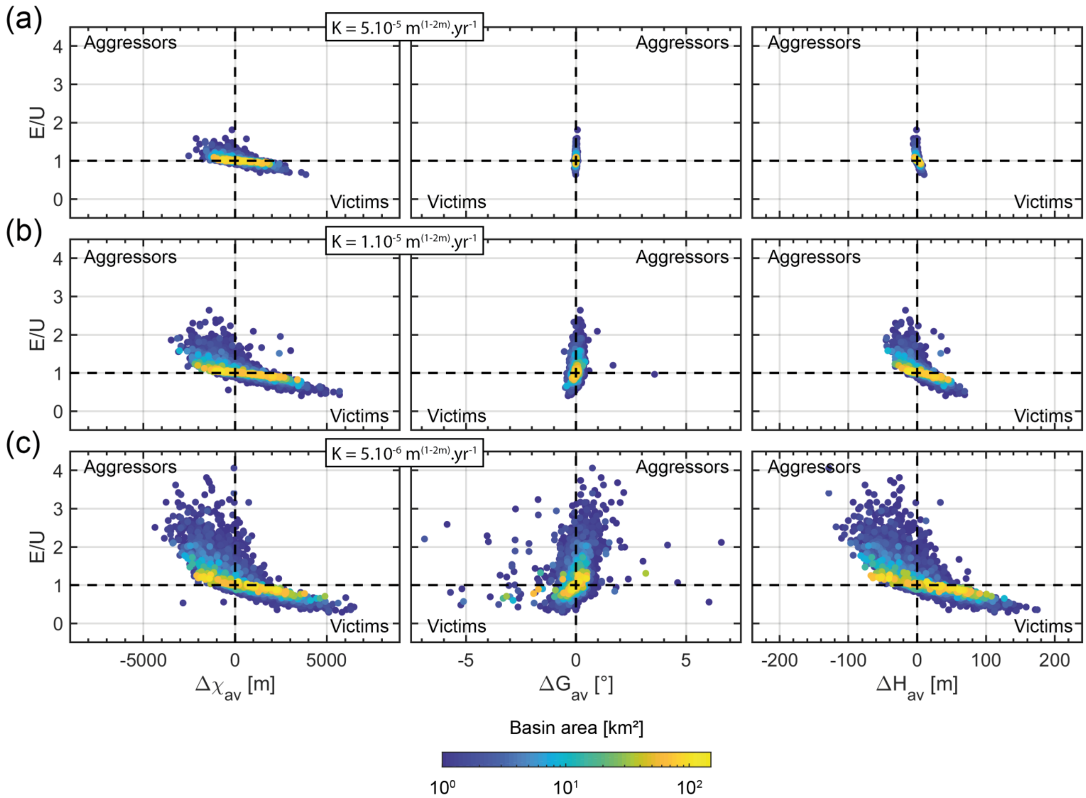

Figure 9: Effect of erodibility. Color scale indicates basin area.

Mis en forme: Anglais (Royaume-Uni)

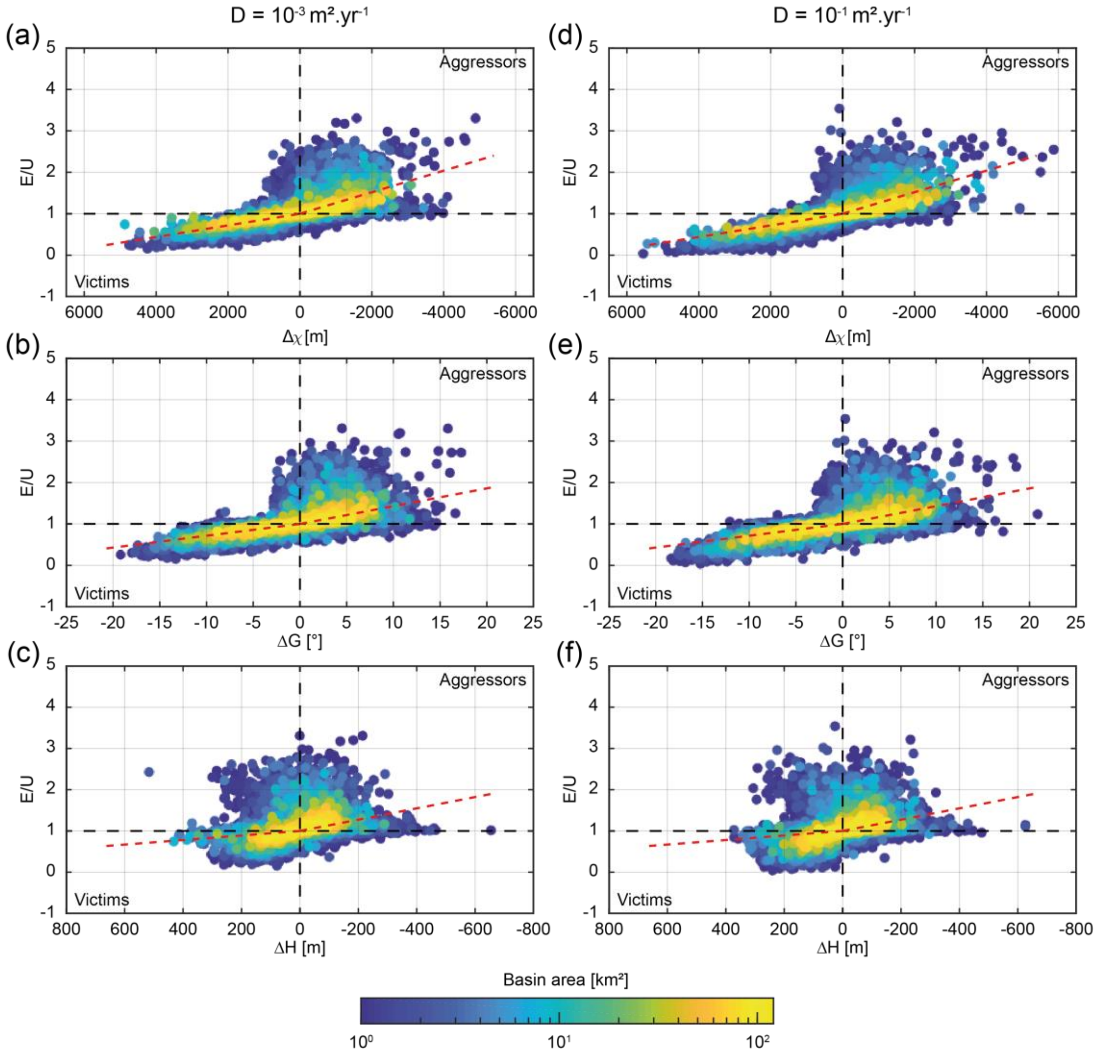

~~**Figure 8:**~~ **Basins of variable sizes, sorted in seven area classes expanding geometrically with a multiplying factor of 2 from 1-2 to 64-128 km², every 0.5 Myr over the time period 5-10 Myr. Basins with a confidence index lower than 50 % are discarded from the analysis. (a) Results with an erodibility coefficient of 5.10^{-5} m$^{(1-2m)}$.yr^{-1}. (b) Results with an erodibility coefficient of 1.10^{-5} m$^{(1-2m)}$.yr^{-1}. (c) Results with an with an erodibility coefficient of 5.10^{-6} m$^{(1-2m)}$.yr^{-1}.**

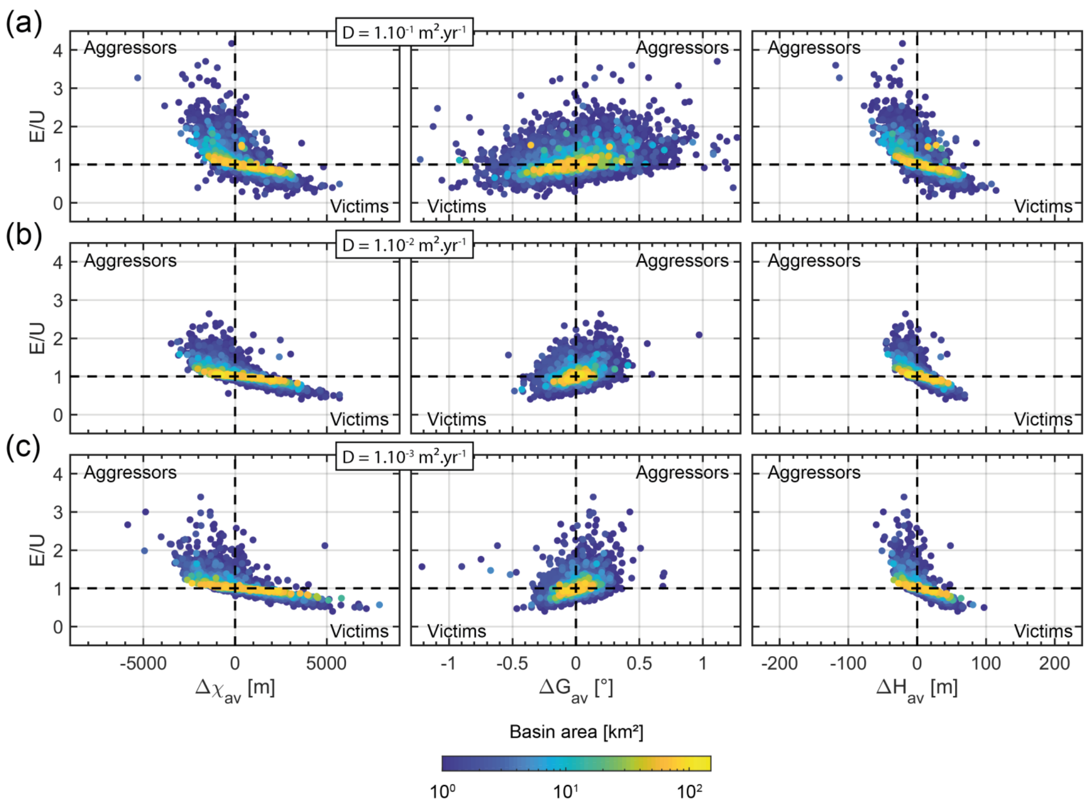

Figure 10: **Effect of diffusivity.** ~~Note that the x-axis is reversed for both $\Delta\chi$ and ΔH~~Color scale indicates basin area. Basins of variable sizes, sorted in seven area classes expanding geometrically with a multiplying factor of 2 from 1-2 to 64-128 km², every 0.5 Myr over the time period 5-10 Myr. Basins with a confidence index lower than 50 % are discarded from the analysis. (a) Results with a diffusivity of 10^{-1} m^2.yr^{-1}. (b) Results with a diffusivity of 10^{-2} m^2.yr^{-1} (~~. Color scale indicates basin area. Red dashed lines correspond to the linear fits obtained for the~~ **reference model** ~~(see figure 6). (a) to (c) Same as Fig. 6d-f~~,). (c) Results **with a diffusivity of 10^{-3} m^2.yr^{-1}**~~. (d) to (f) Same as Fig. 6d-f, with a diffusivity of 10^{-1} m^2.yr^{-1}~~.

Mis en forme: Anglais(Royaume-Uni)

Mis en forme: Anglais(Royaume-Uni)

Mis en forme: Anglais(Royaume-Uni)

Mis en forme: Anglais(Royaume-Uni)

Mis en forme: Anglais(Royaume-Uni)

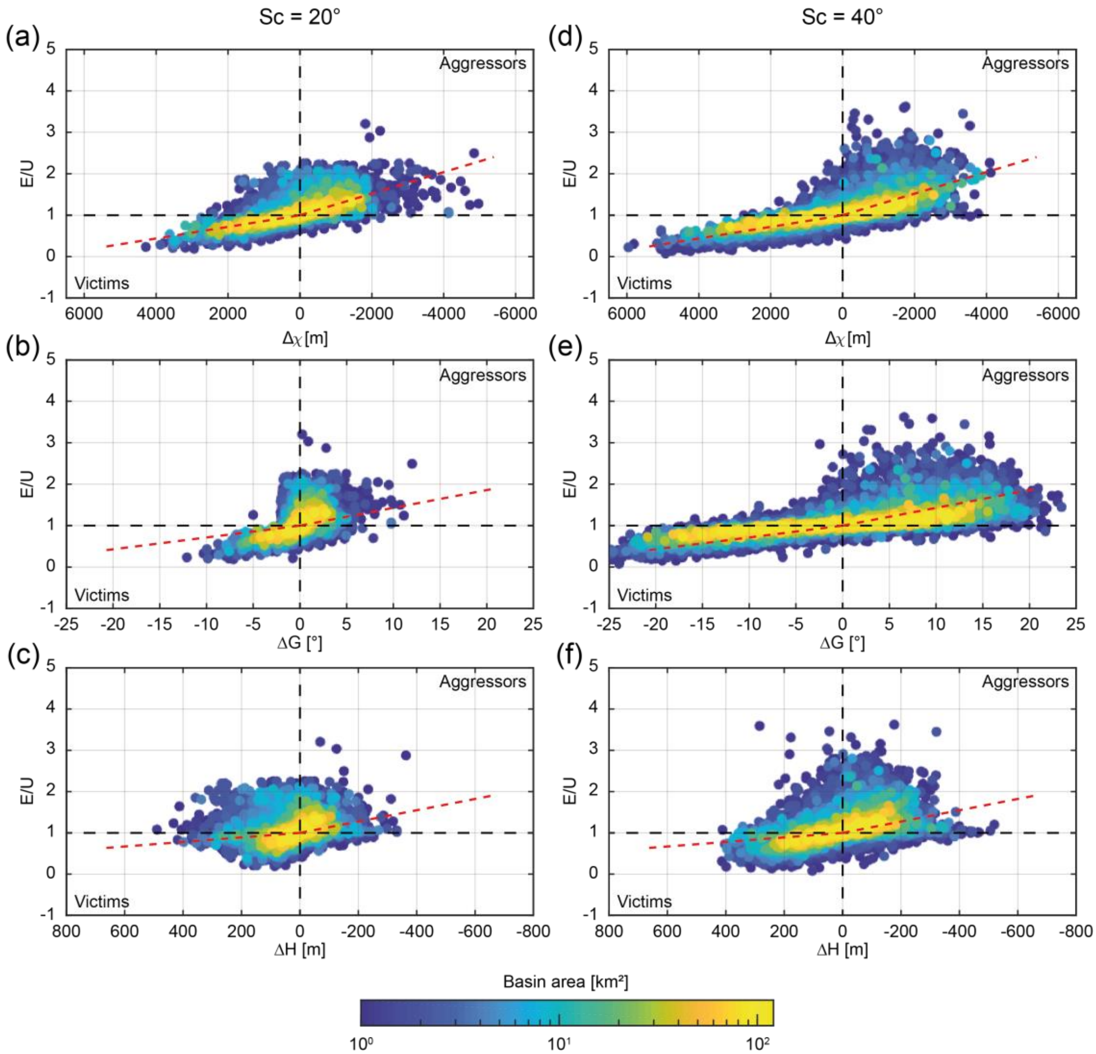
Sc = 20°
Sc = 40°
(a)
(b)
(c)
(d)
(e)
(f)
Aggressors
Victims
E/U
Δχ [m]
ΔG [°]
ΔH [m]
Basin area [km²]
10⁰
10¹
10²

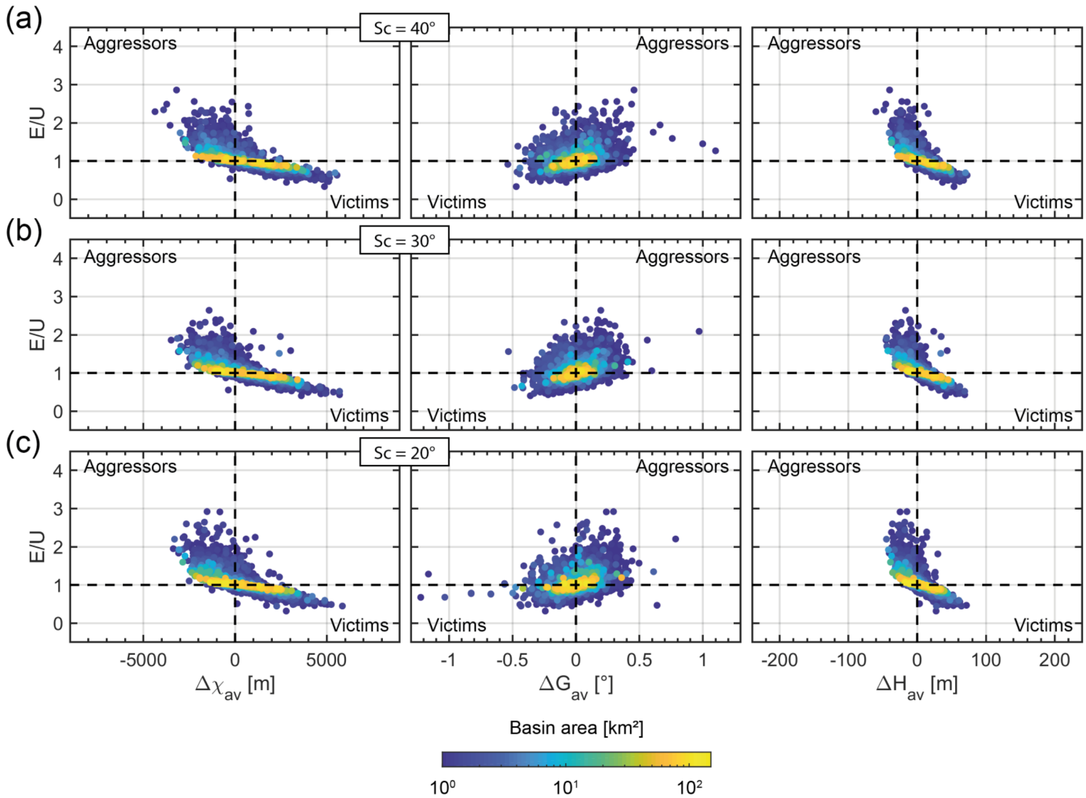

Figure ~~9~~11: Effect of critical slope. ~~Note that the x axis is reversed for both $\Delta\chi$ and ΔH.~~ Color scale indicates basin area. ~~Red dashed lines correspond to~~ Basins of variable sizes, sorted in seven area classes expanding geometrically with a multiplying factor of 2 from 1-2 to 64-128 km², every 0.5 Myr over the time period 5-10 Myr. Basins with a confidence index lower than 50 % are discarded from the ~~linear fits obtained for the~~ analysis. (a) Results with a critical slope of 40°. (b) Results with a critical slope of 30° (reference model ~~(see figure 6). (a) to~~), (c) ~~Same as Fig. 6d-f,~~Results with a critical slope of 20°~~. (d) to (f) Same as Fig. 6d-f, with a critical slope of 40~~°.

Mis en forme: Anglais(Royaume-Uni)
Mis en forme: Anglais(Royaume-Uni)
Mis en forme: Anglais(Royaume-Uni)
Mis en forme: Anglais(Royaume-Uni)
Mis en forme: Anglais(Royaume-Uni)
Mis en forme: Anglais(Royaume-Uni)
Mis en forme: Anglais(Royaume-Uni)
Mis en forme: Anglais(Royaume-Uni)

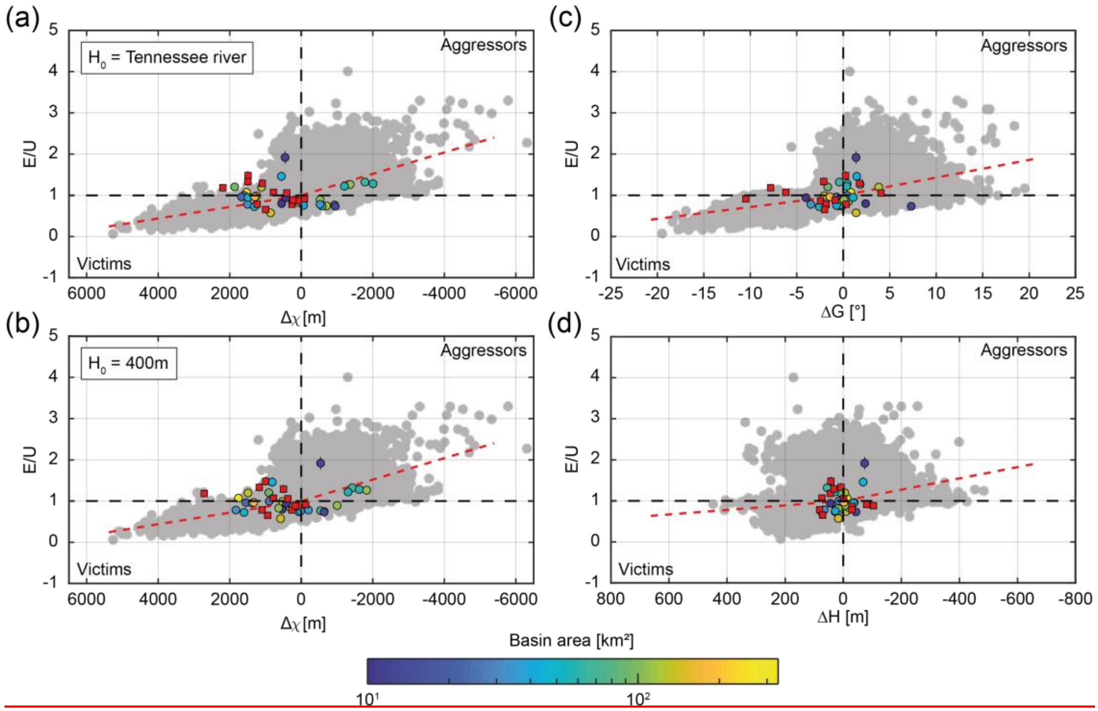
(a)
H_0 = Tennessee river
Aggressors
Victims
E/U
Δχ [m]
(b)
H_0 = 400m
Aggressors
Victims
E/U
Δχ [m]
(c)
Aggressors
Victims
E/U
ΔG [°]
(d)
Aggressors
Victims
E/U
ΔH [m]
Basin area [km²]
10^1
10^2

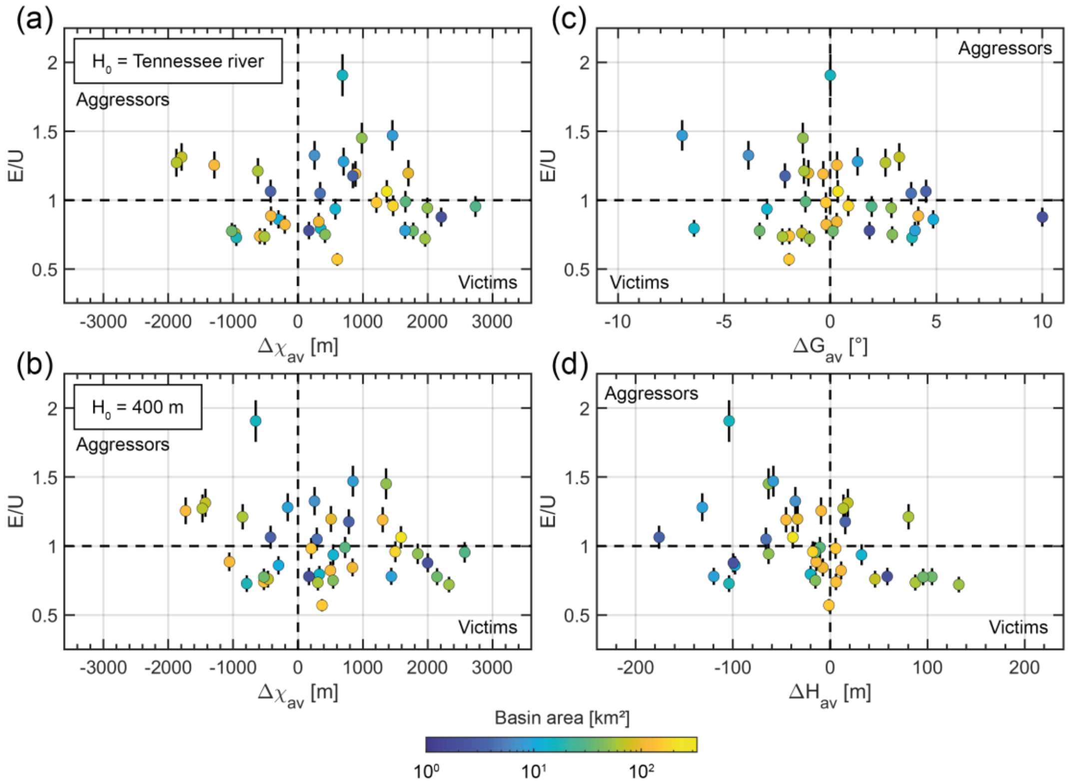

Figure ~~10: Denudation~~12: Normalized denudation rates in the Great Smoky Mountains as a function of aggressivity metrics. ~~Note that the x axis is reversed for both $\Delta\chi$ and ΔH. Color circles are reported according to the E/U ratio for basins sampled by~~Original dataset from Matmon et al.~~, .~~ (2003b~~,~~) with E recalculated by Portenga et al~~., 2011, error~~. (2011). Denudation rates and uncertainties are normalised by the estimated background uplift rate in this region of 0.03 mm.yr^{-1}. Error bars are represented with thin black line~~ but are almost always smaller than symbols.~~. Color scale ~~of these circles is related to~~indicates basin size. ~~Red squares are basins with an area less than 10 km². Red dashed lines correspond to linear fits obtained for the reference model. Grey circles in the background correspond to the reference model (see figure 6).~~ (a) and (b) Relationship between denudation rates and ~~$\Delta\chi$~~$\Delta\chi_{av}$ with a base level corresponding to the Tennessee river and at a fixed elevation of 400 m, respectively. (c) and (d) Relationship between denudation rates and ~~Gilbert~~Gilbert's aggressivity metrics, ~~ΔG~~ΔG_{av} and ~~ΔH,~~ΔH_{av}~~;~~, respectively.

Mis en forme: Anglais(Royaume-Uni)
Mis en forme: Anglais(Royaume-Uni)
Mis en forme: Anglais(Royaume-Uni)
Mis en forme: Anglais(Royaume-Uni)
Mis en forme: Anglais(Royaume-Uni)
Mis en forme: Anglais(Royaume-Uni)
Mis en forme: Anglais(Royaume-Uni)
Mis en forme: Anglais(Royaume-Uni)
Mis en forme: Anglais(Royaume-Uni)
Mis en forme: Anglais(Royaume-Uni)
Mis en forme: Anglais(Royaume-Uni)
Mis en forme: Anglais(Royaume-Uni)
Mis en forme: Anglais(Royaume-Uni)
Mis en forme: Anglais(Royaume-Uni)

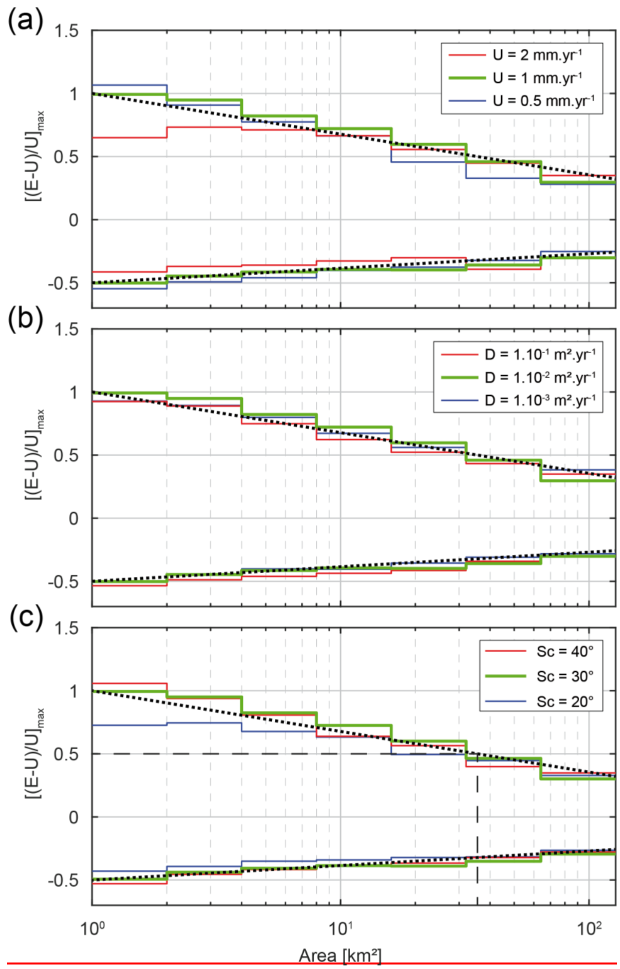

(a)
(b)
(c)
[(E-U)/U]max
U = 2 mm.yr-1
U = 1 mm.yr-1
U = 0.5 mm.yr-1
D = 1.10-1 m².yr-1
D = 1.10-2 m².yr-1
D = 1.10-3 m².yr-1
Sc = 40°
Sc = 30°
Sc = 20°
1.5
1
0.5
0
-0.5
10^0
10^1
10^2
Area [km²]

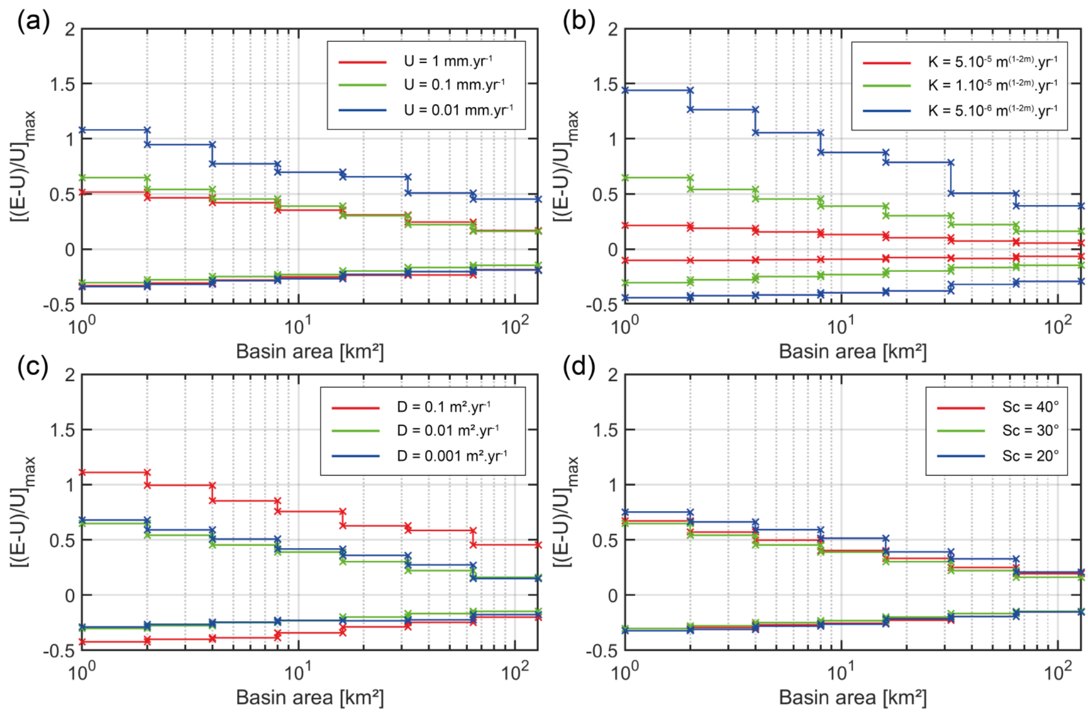

Figure ~~11~~13: Deviation from steady state due to drainage migration as a function of basin size. Color lines ~~are related to~~show the maximum dispersion of denudation rates (0.5 and 99.5 percentiles) due to divide mobility. Green lines ~~are associated with the results obtained for the reference model. Dotted black lines represent the logarithm relationship between $[(E-U)/U]_{max}$ and the basin area for victim and aggressor watersheds (Eq.7).~~indicate the reference model. Seven sets of basin size are considered: 1-2, 2-4, 4-8, 8-16, 16-32, 32-64 and 64-128 km² every 0.5 Myr between ~~2.~~5 and 10 Myr. (a) Effect of uplift rate. (b) Effect of ~~diffusivity~~erodibility. (c) Effect of diffusivity. (d) Effect of critical slope. ~~Thin dashed black lines show the minimal basin area required for a maximal denudation rate deviation from uplift rate equal to 0.5.~~

Mis en forme: Anglais(Royaume-Uni)
Mis en forme: Anglais(Royaume-Uni)
Mis en forme: Anglais(Royaume-Uni)
Mis en forme: Anglais(Royaume-Uni)
Mis en forme: Anglais(Royaume-Uni)
Mis en forme: Anglais(Royaume-Uni)
Mis en forme: Anglais(Royaume-Uni)
Mis en forme: Anglais(Royaume-Uni)
Mis en forme: Légende